



Static Bending Behaviour of FG-CNTRC Microbeams Resting on Elastic Foundation Using Higher-Order Shear Deformation Beam Theories and Modified Couple Stress Theory

Van-Hieu Dang^{*}

Faculty of Mechanical Engineering and Mechatronics, Phenikaa University, 12116 Hanoi, Vietnam

^{*} Correspondence: Van-Hieu Dang (hieu.dangvan@phenikaa-uni.edu.vn)**Received:** 06-15-2025**Revised:** 08-10-2025**Accepted:** 08-25-2025

Citation: V. H. Dang, "Static bending behaviour of FG-CNTRC microbeams resting on elastic foundation using higher-order shear deformation beam theories and modified couple stress theory," *Math. Model. Sustain. Eng.*, vol. 1, no. 1, pp. 1–25, 2025. <https://doi.org/10.56578/mmse010101>.



© 2025 by the author(s). Licensee Acadlore Publishing Services Limited, Hong Kong. This article can be downloaded for free, and reused and quoted with a citation of the original published version, under the CC BY 4.0 license.

Abstract: This study investigated the static bending behavior of functionally graded carbon nanotube-reinforced composite (FG-CNTRC) microbeams supported on an elastic foundation. The proposed model was formulated by coupling higher-order shear deformation beam theories (HoSDBTs) with the modified couple stress theory (MCST). Four distinct CNT distribution patterns within the polymer matrix were considered. Using Hamilton's principle, governing equations and boundary conditions for simply-supported microbeams were derived and solved analytically. This comprehensive parametric study explored the effects of the material length scale, CNT volume fraction, aspect ratio, foundation stiffness (Winkler and Pasternak models), and CNT gradation on bending stiffness. Results revealed that all parameters notably influenced the mechanical response, with key roles played by size-dependent effects and elastic foundation interactions. The proposed MCST-enhanced HoSDBT model effectively captures size-dependent behaviors, rendering it suitable for the design and optimization of FG-CNTRC micro-devices.

Keywords: Microbeams; Modified couple stress theory; Shear deformation beam; Functionally graded; Carbon nanotubes

1 Introduction

The rapid advancement of micro- and nano-scale structures has profoundly influenced modern engineering and technology. Microelectromechanical systems (MEMS) and nanoelectromechanical systems (NEMS) have become essential components in diverse applications such as sensors, actuators, biomedical devices, and communication systems [1–3]. These systems offer distinct advantages, including miniaturization, high sensitivity, low power consumption, and compatibility with large-scale integration. Progress in micro/nanofabrication techniques has enabled precise control at extremely small scales, leading to devices with superior mechanical performance and higher operational frequencies [4]. Understanding the mechanical behavior of MEMS and NEMS is crucial to ensure their reliability and optimal performance; at such small scales, effects such as surface forces, thermal fluctuations, and size-dependent material properties play dominant roles [5–7].

Functionally graded materials (FGMs) are advanced composites distinguished by a gradual variation in composition and microstructure across their volume, resulting in corresponding changes in mechanical, thermal, and physical properties [8, 9]. This smooth gradation enables FGMs to achieve tailored property distributions that meet specific functional requirements, effectively mitigating stress concentrations or interfacial failures typically associated with abrupt material transitions [10]. At micro- and nano-scales, FGMs provide notable advantages. Their graded characteristics can be engineered to enhance stiffness, thermal stability, and durability of microbeams and miniature components [11, 12]. Shariati et al. [13] studied how non-uniform material distribution in a viscoelastic, axially-moving Rayleigh beam affects its vibration behavior and stability, deriving exact critical velocities and mapping divergence and flutter instability regions. A refined high-order shear deformation theory was proposed by Hadji et al. [14] to analyze the static bending of functionally graded sandwich plates, showing how material gradation, lay-up, and aspect ratio influence deflections and stresses. Rizov [15] analyzed how delamination in U-shaped, multilayered viscoelastic FG structures influences the strain energy release rate, using equilibrium equations and the J-integral to explore the effect of material gradients and support conditions.

Functionally graded carbon nanotube-reinforced composites (FG-CNTRCs) have emerged as a novel class of nanomaterials engineered to optimize the outstanding mechanical, thermal, and electrical properties of carbon nanotubes (CNTs) within composite structures [16, 17]. By varying the distribution of CNTs across the thickness of the polymer matrix, FG-CNTRCs can achieve optimized mechanical, thermal, and electrical properties tailored for specific engineering applications. Typical CNT distribution patterns include uniform distribution (UD), “V-shaped” distribution (FG-V), “O-shaped” distribution (FG-O), and “X-shaped” distribution (FG-X) [17].

Extensive research has been devoted to analyzing the mechanical responses of FG-CNTRC beams under different environments [18–23]. With the rapid advancement of MEMS/NEMS technologies, it has become evident that classical continuum mechanics fails to accurately predict the mechanical behavior of micro- and nano-scale structures [24–27]. To address these scale-dependent deviations, various higher-order continuum theories were developed [28–33]. Thai et al. [34] reviewed advanced continuum mechanics theories—including nonlocal elasticity, modified couple stress, and strain-gradient models—used to capture size effects in small-scale beams and plates, and discusses their finite-element implementations and future directions. Ebrahimi and Barati [35] developed a nonlocal, third-order shear deformation beam model to study how size effects and material gradation influence the free vibration frequencies of functionally graded nanobeams. Shariati et al. [36] investigated how axial gradation, nonlocal effects, and viscoelastic damping influence the vibration characteristics and stability (divergence and flutter) of moving AFG nanobeams, showing that proper material distribution can significantly improve stability. Kong [37] reviewed size-dependent modelling of micro-beams and micro-plates based on Modified Couple Stress Theory (MCST), emphasising how the inclusion of a material length-scale parameter alters bending, buckling, vibration and pull-in instability predictions compared to classical theories. Simsek and Reddy [38] proposed a new higher-order beam theory coupled with modified couple stress theory to analyze the static bending and free vibration of functionally graded micro-beams, revealing significant size-dependency effects via a material length-scale parameter. Ke and Wang [39] investigated how micro-scale size effects, via the modified couple stress theory, influence the dynamic stability (e.g. parametric resonance) of functionally graded microbeams. A size-dependent Euler–Bernoulli beam model was developed by Gorji Azandariani et al. [40] using modified couple stress theory to perform a nonlinear static analysis of a bidirectional functionally graded microbeam on a nonlinear elastic foundation, revealing how gradient indices, length-scale parameter, and foundation stiffness significantly affect its deflection. Wattanasakulpong et al. [41] investigated how size-dependent effects (via modified couple stress theory) influence the vibration behavior of functionally graded sandwich microbeams under different boundary conditions, showing that microscale stiffness increases, raising natural frequencies. Shenas et al. [42] presented a unified higher-order beam theory based on a stress–strain gradient framework to analyze free vibration and buckling of CNT-reinforced functionally graded microbeams embedded in an elastic medium, highlighting how nonlocal effects, CNT distribution, and foundation stiffness influence stability and natural frequencies. The nonlinear dynamic behavior of non-uniform microscale composite beams reinforced with CNTs, incorporating size effects through the modified couple stress theory and geometric nonlinearity was investigated by Alimoradzadeh et al. [43].

To the best of our knowledge, this study represents the first comprehensive analytical investigation that integrates the modified couple stress theory (MCST) with high-order shear deformation beam theories (HoSDBTs) to model static bending of FG-CNTRC microbeams resting on an elastic foundation under simply-supported boundary conditions. This paper introduces four distinct CNT distribution patterns, derives governing equations and boundary conditions via Hamilton’s Principle, and presents exact analytical solutions for these configurations. The objectives of this study are to: (1) define the material properties of the functionally-graded carbon-nanotube-reinforced composite (FG-CNTRC); (2) formulate the governing equations based on the modified couple stress theory (MCST) together with the high-order shear deformation beam theory (HoSDBT); and (3) apply the developed formulation to perform static bending analysis of FG-CNTRC microbeams.

Despite the analytical rigor of the current model, some limitations must be acknowledged. First, only simply-supported (S-S) boundary conditions were considered but these might not reflect the full range of realistic support conditions encountered in MEMS/NEMS devices (e.g., clamped, free-clamped, and mixed). Second, the model assumes perfect alignment, dispersion, and bonding of carbon nanotubes (CNTs) within the FG-CNTRC matrix and neglects the effects of CNT agglomeration, interface debonding or micro-defects, which could degrade the mechanical performance in practice. Third, the elastic foundation was modelled with simplified assumptions (e.g., linear Winkler/Pasternak behavior) and did not account for possible nonlinear, time-dependent or substrate-microstructure interaction phenomena. Finally, size-dependent effects were captured via the selected higher-order shear deformation theory and modified couple stress theory, but other effects such as surface energy, residual stresses, roughness, and manufacturing imperfections are outside the scope of this study as these may become significant at extreme micro-/nano-scales.

2 Functionally Graded Carbon Nanotube-Reinforced Composite

As illustrated in Figure 1, an FG-CNTRC microbeam resting on an elastic foundation and subject to a transverse distributed load has been considered in this study. The microbeam has a rectangular cross-section with length L , width b , and thickness h . A Cartesian coordinate system $Oxyz$ is defined such that the x -axis coincides with the longitudinal axis of the microbeam, the y -axis corresponds to the width direction, and the z -axis represents the thickness direction. The origin O is located at the mid-point of the left end of the microbeam. The microbeam is simply supported at both ends and subject to a transverse distributed load $q(x)$ acting in the z -direction, which may vary spatially. To model the interaction between the microbeam and its supporting medium, a two-parameter Winkler–Pasternak foundation model was employed. The Winkler component provides a linear elastic reaction proportional to the local deflection $w(x)$ through the modulus k_w while the Pasternak shear layer introduces a shear modulus k_p that accounts for transverse shear interactions between adjacent points in the foundation.

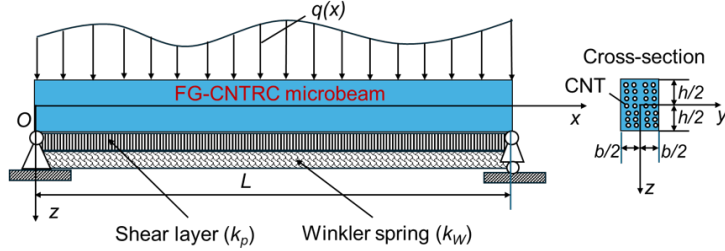


Figure 1. Geometry of an FG-CNTRC microbeam resting on an elastic foundation

The FG-CNTRC microbeam is composed of a polymer matrix reinforced with carbon nanotubes (CNTs). Unlike conventional composites with uniformly distributed reinforcements, the CNT volume fraction in the FG-CNTRC microbeam varies continuously along the thickness direction, z -axis, according to predefined distribution patterns such as uniform (UD), V-shaped (FG-V), O-shaped (FG-O), and X-shaped (FG-X) profiles. These four CNT distribution patterns, as illustrated in Figure 2, demonstrate the functionally graded nature of the composite structure. Such gradation enables tailored mechanical performance by enhancing stiffness, strength, and resistance to buckling and vibration. The CNTs are assumed to be perfectly bonded to the polymer matrix and uniformly dispersed in the in-plane directions, with the volume fraction varying only through the thickness. The effective material properties, namely Young's modulus, shear modulus, Poisson's ratio, and density were evaluated using the extended rule of mixtures, which introduces CNT efficiency parameters to account for nanoscale effects, load-transfer mechanisms, and interfacial interactions. This micromechanical approach ensures accurate characterization of the composite behavior, particularly when structural dimensions reach the microscale. Based on the extended rule of mixtures, the effective Young's moduli (E_{11} , E_{22}) and shear modulus (G_{12}) of the FG-CNTRC microbeam are expressed [16–23]:

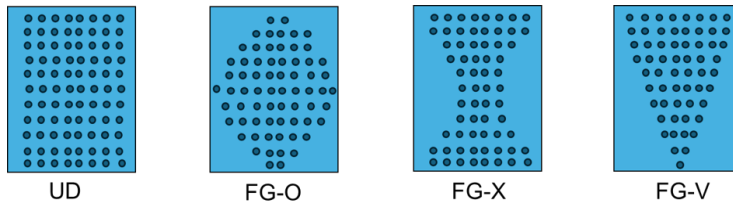


Figure 2. Four different CNT distribution patterns

$$E_{11}(z) = \eta_1 V_{CNT}(z) E_{11}^{CNT} + V_m(z) E^m \quad (1)$$

$$\frac{\eta_2}{E_{22}(z)} = \frac{V_{CNT}(z)}{E_{22}^{CNT}} + \frac{V_m(z)}{E^m} \quad (2)$$

$$\frac{\eta_3}{G_{12}(z)} = \frac{V_{CNT}(z)}{G_{12}^{CNT}} + \frac{V_m(z)}{G^m} \quad (3)$$

where, E_{11}^{CNT} and E_{22}^{CNT} denote the longitudinal and transverse Young's moduli of CNTs, respectively, and G_{12}^{CNT} represents their shear modulus. The isotropic polymer matrix possesses Young's modulus E^m and shear modulus G^m . In modeling FG-CNTRC materials, efficiency parameters (η_1 , η_2 , and η_3) are introduced as correction factors to bridge the gap between idealized micromechanical predictions and the actual behavior of nanocomposites. These parameters account for nanoscale imperfections and complexities such as CNT waviness, partial alignment, interfacial debonding, and non-uniform dispersion within the polymer matrix. Because conventional rule-of-mixture formulations often overestimate stiffness by assuming perfect bonding and uniform stress transfer, the efficiency parameters serve to appropriately scale the CNT contribution in the longitudinal, transverse, and shear directions. Their values are typically determined through molecular dynamic simulations, experimental calibration, or inverse modeling techniques, and they play a crucial role in achieving realistic estimations of effective material properties in FG-CNTRCs. The volume fractions of CNTs (V_{CNT}) and the polymer matrix (V_m) are related by [16–23]:

$$V_{CNT}(z) + V_m(z) = 1 \quad (4)$$

which guarantees that at each point through the thickness, the composite is fully occupied by the two constituent phases.

For the UD case, the CNTs are uniformly dispersed through the thickness of the microbeam, so the local volume fraction of CNTs at coordinate z is equal to the overall volume fraction of CNTs, V_{CNT}^* , as shown below [16–23]:

$$V_{CNT}(z) = V_{CNT}^* \quad (5)$$

For the FG-O, FG-X, and FG-V distributions, the CNT volume fraction V_{CNT} along the thickness direction z can be expressed as follows [16–23]:

$$V_{CNT}(z) = f(z) \cdot V_{CNT}^* \quad (6)$$

where, $f(z)$ defines the distribution profile of CNTs through the thickness coordinate z . For each graded distribution pattern of CNTs, the corresponding shape function $f(z)$ is specified as follows [16–23]:

$$f(z) = \begin{cases} 2 - \frac{4|z|}{h} & \text{for FG-O} \\ \frac{4|z|}{h} & \text{for FG-X} \\ 1 + \frac{2z}{h} & \text{for FG-V} \end{cases} \quad (7)$$

From Eqs. (5)–(7), the CNT volume fraction, V_{CNT} , for the four distribution types can be written as follows:

$$V_{CNT}(z) = \begin{cases} V_{CNT}^* & \text{for UD} \\ \left(2 - \frac{4|z|}{h}\right) \cdot V_{CNT}^* & \text{for FG-O} \\ \left(\frac{4|z|}{h}\right) \cdot V_{CNT}^* & \text{for FG-X} \\ \left(1 + \frac{2z}{h}\right) \cdot V_{CNT}^* & \text{for FG-V} \end{cases} \quad (8)$$

Figure 3 shows the variation of the effective Young's moduli (E_{11} , E_{22}) and the shear modulus (G_{12}) of the FG-CNTRC microbeam to the normalized thickness (z/h) for the case of $V_{CNT}^* = 0.12$. The total volume fraction of CNTs, V_{CNT}^* , is defined as [16–23]:

$$V_{CNT}^* = \frac{w_{CNT}}{w_{CNT} + (\rho^{CNT}/\rho^m) - (\rho^{CNT}/\rho^m) w_{CNT}} \quad (9)$$

In this expression, w_{CNT} denotes the mass fraction of CNTs, to represent the overall or average volume fraction of CNTs in the composite microbeam. ρ^{CNT} and ρ^m are the mass densities of the CNTs and the isotropic polymer matrix, respectively. No efficiency parameters are required to adjust the Poisson's ratios (v_{12} , v_{21}) of the FG-CNTRC microbeam which are estimated as follows [16–23]:

$$v_{12}(z) = V_{CNT}(z)v_{12}^{CNT} + V_m(z)v^m \quad (10)$$

$$v_{21}(z) = \frac{v_{12}(z)}{E_{11}(z)} E_{22}(z) \quad (11)$$

where, v_{12}^{CNT} and v^m denote the Poisson's ratios of the CNTs and the polymer matrix, respectively. The effective elastic and shear moduli are then calculated as follows [19]:

$$E(z) = \frac{E_{11}(z)}{1 - v_{12}(z)v_{21}(z)}, G(z) = G_{12}(z) \quad (12)$$

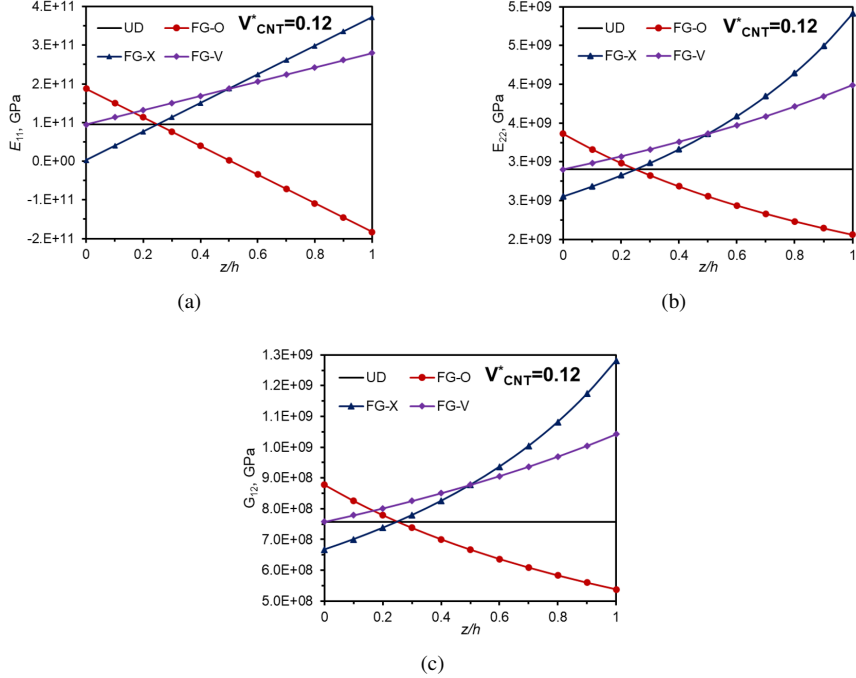


Figure 3. Effective Young's Moduli (E_{11}, E_{22}) and Shear Modulus (G_{12}) of the FG-CNTRC Microbeam

3 Modified Couple Stress Theory

According to the MCST introduced by Yang et al. [32], the strain energy density of a linear, elastic, and isotropic material depends not only on the classical strain tensor energetically conjugates to the Cauchy stress tensor but also on the symmetric curvature tensor, which conjugates to the deviatoric part of the couple-stress tensor. The inclusion of a material length scale parameter (l) enables the MCST to capture size-dependent mechanical behavior at the microscale. Consequently, the total strain energy stored in a deformed body of volume V can be expressed as [32]:

$$U_s = \frac{1}{2} \int_V (\sigma_{ij}\varepsilon_{ij} + m_{ij}\chi_{ij}) dV, \quad (i, j = 1, 2, 3) \quad (13)$$

where, σ_{ij} and ε_{ij} denote the Cauchy stress tensor and the strain tensor, respectively; m_{ij} is the deviatoric part of the couple stress tensor, and χ_{ij} is the symmetric curvature tensor. These tensors are mathematically defined as follows [32]:

$$\sigma_{ij} = \lambda \text{tr}(\varepsilon_{ij}) I + 2\mu\varepsilon_{ij} \quad (14)$$

$$\varepsilon_{ij} = \frac{1}{2} \left[\frac{\partial u_i}{\partial x_j} + \frac{\partial u_j}{\partial x_i} \right] \quad (15)$$

$$m_{ij} = 2\mu l^2 \chi_{ij} \quad (16)$$

$$\chi_{ij} = \frac{1}{2} \left[\frac{\partial \theta_i}{\partial x_j} + \frac{\partial \theta_j}{\partial x_i} \right] \quad (17)$$

where, u_i are denoted for the components of the displacement vector, λ and μ denote the Lamé constants of the isotropic material, I is the identity tensor, and θ_i are the components of the rotation vector, which can be expressed in terms of the displacement field as [32]:

$$\theta_i = \frac{1}{2} \operatorname{curl}(u_i) \quad (18)$$

4 Equilibrium Equations

A unified higher-order shear deformation beam theory was adopted in this study, in order to precisely model the mechanical behavior of FG-CNTRC microbeams. This unified framework consolidates various shear deformation theories into a single formulation, which enables it to capture both transverse shear deformation and normal-strain effects without the need for shear-correction factors. By introducing higher-order terms in the displacement field, the formulation attains greater accuracy compared to classical and first-order theories, particularly when analyzing thick microbeams and size-dependent phenomena governed by the modified couple-stress theory. According to this theory, the displacement components are expressed as [38]:

$$u_x(x, z) = u(x) - z \frac{\partial w(x)}{\partial x} + g(z)\gamma(x) \quad (19)$$

$$u_y(x, z) = 0 \quad (20)$$

$$u_z(x, z) = w(x) \quad (21)$$

where, $u(x)$ and $w(x)$ are denoted for the axial and transverse displacement of any point on the neutral axis of the FG-CNTRC microbeam, respectively; $\gamma(x)$ denotes the higher-order rotation related to transverse shear deformation of any point on the neutral axis of the microbeam. The higher-order rotation $\gamma(x)$ can be expressed as [38]:

$$\gamma(x) = \frac{\partial w(x)}{\partial x} - \phi(x) \quad (22)$$

where, the linear rotation term $\phi(x)$ accounts for the bending of the cross-section at any point on the neutral axis. The presence of the higher-order shear deformation term $g(z)\gamma(x)$ is essential for capturing the non-linear variation of shear strains through the thickness. The through-thickness shape function $g(z)$ is specifically chosen so that the traction-free boundary conditions at the top and bottom surfaces of the microbeam are satisfied. The particular expressions of $g(z)$ for different higher-order beam theories are summarized in Table 1.

By substituting the displacement field defined in Eq. (19) to Eq. (21) into Eq. (15), the individual components of the strain tensor are derived as follows:

$$\varepsilon_{xx} = \frac{\partial u}{\partial x} - z \frac{\partial^2 w}{\partial x^2} + g(z) \frac{\partial \gamma}{\partial x}, \quad (23)$$

$$\gamma_{xz} = 2\varepsilon_{xz} = \frac{\partial g}{\partial z} \gamma, \quad (24)$$

$$\varepsilon_{yy} = \varepsilon_{zz} = \gamma_{xy} = \gamma_{yz} = 0. \quad (25)$$

Table 1. Shape function $g(z)$ for different higher-order beam theories [38]

Beam Theory	Shape Function
Euler–Bernoulli beam theory (EBBT)	$g(z) = 0$
First-order shear deformation beam theory (FSDBT)	$g(z) = z$
Parabolic shear deformation beam theory (PSDBT)	$g(z) = z(1 - 4z^2/3h^2)$
Trigonometric shear deformation beam theory (TSDBT)	$g(z) = \frac{h}{\pi} \sin\left(\frac{\pi z}{h}\right)$
Hyperbolic shear deformation beam theory (HSDBT)	$g(z) = h \sinh\left(\frac{z}{h}\right) - z \cosh\left(\frac{1}{2}\right)$
Exponential shear deformation beam theory (ESDBT)	$g(z) = ze^{-2(z/h)^2}$
Aydogdu shear deformation beam theory (ASDBT)	$g(z) = z^3 e^{\frac{-2(z/h)^2}{\ln 3}}$

By applying Eq. (18) and Eqs. (19)–(21), the components of the rotation vector can be written as follows:

$$\theta_x = 0, \theta_y = \frac{1}{2} \frac{\partial g}{\partial z} \gamma - \frac{\partial w}{\partial x}, \theta_z = 0. \quad (26)$$

Substituting Eq. (26) into Eq. (17), the components of the symmetric curvature tensor can be obtained as:

$$\chi_{xy} = \frac{1}{4} \frac{\partial g}{\partial z} \frac{\partial \gamma}{\partial x} - \frac{1}{2} \frac{\partial^2 w}{\partial x^2}, \quad (27)$$

$$\chi_{yz} = \frac{1}{4} \frac{\partial^2 g}{\partial z^2} \gamma \quad (28)$$

$$\chi_{xx} = \chi_{yy} = \chi_{zz} = \chi_{xz} = 0. \quad (29)$$

In this study, the governing equations of motion are derived in a systematic way using Hamilton's principle, which provides a variational framework for dynamic equilibrium. Mathematically, this principle is stated as:

$$\int_{t_1}^{t_2} (\delta W_e - \delta U_s - \delta U_f) dt = 0 \quad (30)$$

where, W_e , U_s , and U_f denote the work done by external forces, the strain energy, and the potential energy of the elastic foundation, respectively. From Eq. (13), the strain energy of the microbeam can be expressed as:

$$\begin{aligned} U_s &= \frac{1}{2} \int_V (\sigma_{xx} \varepsilon_{xx} + 2\sigma_{xz} \varepsilon_{xz} + 2m_{xy} \chi_{xy} + 2m_{yz} \chi_{yz}) dV \\ &= \frac{1}{2} \int_0^L \int_A \left\{ \sigma_{xx} \left(\frac{\partial u}{\partial x} - z \frac{\partial^2 w}{\partial x^2} + g(z) \frac{\partial \gamma}{\partial x} \right) + \sigma_{xz} \frac{\partial g(z)}{\partial z} \gamma \right. \\ &\quad \left. + m_{xy} \left[\frac{1}{2} \frac{\partial g(z)}{\partial z} \frac{\partial \gamma}{\partial x} - \frac{\partial^2 w}{\partial x^2} \right] + \frac{1}{2} m_{yz} \frac{\partial^2 g(z)}{\partial z^2} \gamma \right\} dA dx \end{aligned} \quad (31)$$

Consequently, the virtual variation of the strain energy can be expressed as:

$$\delta U_s = \frac{1}{2} \int_0^L \left[N_{xx} \frac{\partial \delta u}{\partial x} - (M_{xx} + P_1) \frac{\partial^2 \delta w}{\partial x^2} + \left(M_{nc} + \frac{1}{2} P_2 \right) \frac{\partial \delta \gamma}{\partial x} + \left(Q + \frac{1}{2} P_3 \right) \delta \gamma \right] dx \quad (32)$$

where,

$$N_{xx} = \int_A \sigma_{xx} dA = A_{11} \frac{\partial u}{\partial x} - B_{11} \frac{\partial^2 w}{\partial x^2} + E_{11} \frac{\partial \gamma}{\partial x} \quad (33)$$

$$M_{xx} = \int_A z \sigma_{xx} dA = B_{11} \frac{\partial u}{\partial x} - D_{11} \frac{\partial^2 w}{\partial x^2} + F_{11} \frac{\partial \gamma}{\partial x} \quad (34)$$

$$M_{nc} = \int_A g(z) \sigma_{xx} dA = E_{11} \frac{\partial u}{\partial x} - F_{11} \frac{\partial^2 w}{\partial x^2} + H_{11} \frac{\partial \gamma}{\partial x} \quad (35)$$

$$Q = \int_A \frac{\partial g(z)}{\partial z} \sigma_{xz} dA = B_{13} \gamma \quad (36)$$

$$P_1 = \int_A m_{xy} dA = \int_A 2\mu(z) l^2 \chi_{xy} dA = \frac{1}{2} D_{13} l^2 \frac{\partial \gamma}{\partial x} - A_{13} l^2 \frac{\partial^2 w}{\partial x^2} \quad (37)$$

$$P_2 = \int_A \frac{\partial g(z)}{\partial z} m_{xy} dA = \int_A 2 \frac{\partial g(z)}{\partial z} \mu(z) l^2 \chi_{xy} dA = \frac{1}{2} B_{13} l^2 \frac{\partial \gamma}{\partial x} - D_{13} l^2 \frac{\partial^2 w}{\partial x^2} \quad (38)$$

$$P_3 = \int_A \frac{\partial^2 g(z)}{\partial z^2} m_{yz} dA = \int_A 2 \frac{\partial^2 g(z)}{\partial z^2} \mu(z) l^2 \chi_{yz} dA = \frac{1}{2} E_{13} l^2 \gamma \quad (39)$$

where,

$$(A_{11}, B_{11}, D_{11}, E_{11}, F_{11}, H_{11}) = b \int_{-h/2}^{h/2} E(z) [1, z, z^2, g(z), zg(z), g^2(z)] dz, \quad (40)$$

$$(A_{13}, D_{13}, E_{13}) = b \int_{-h/2}^{h/2} G(z) \left[1, \frac{\partial g(z)}{\partial z}, \left(\frac{\partial^2 g(z)}{\partial z^2} \right)^2 \right] dz \quad (41)$$

$$B_{13} = b k_s \int_{-h/2}^{h/2} G(z) \left(\frac{\partial g(z)}{\partial z} \right)^2 dz \quad (42)$$

Here, k_s denotes the shear correction factor. This factor is introduced to compensate for the discrepancy between the assumed and actual shear-strain energy distributions across the microbeam's thickness. For first-order shear deformation beam theory (FSDBT), a constant shear strain is assumed and leads to an overestimation of shear stiffness, hence a commonly accepted value of $k_s = 5/6$ adopted for FSDBT. In contrast, for higher-order shear deformation beam theories (HoSDBTs) such as PSDBT, TSDBT, HSDBT, ESDBT, and ASDBT, the assumed displacement fields more accurately represent the parabolic variation of shear strains and satisfy the traction-free boundary conditions on the top and bottom surfaces. Therefore, the shear correction factor is typically taken as $k_s = 1$. The virtual potential energy of the elastic foundation can be expressed as:

$$\delta U_f = \int_0^L \left(k_w w \delta w + k_p \frac{\partial w}{\partial x} \frac{\partial \delta w}{\partial x} \right) dx \quad (43)$$

The virtual work done by external force, including the transverse distributed load $q(x)$, is given by:

$$\delta W_e = \int_0^L q(x) \delta w dx \quad (44)$$

By substituting the expressions for the virtual variation of strain energy from Eq. (32), the virtual potential energy of the elastic foundation from Eq. (43), and the virtual work done by external force from Eq. (44) into Hamilton's principle in Eq. (30), then performing integration by parts and collecting the coefficients of the generalized displacements δu , δw and $\delta \gamma$, this study obtains the equilibrium equations for the FG-CNTRC microbeam based on the MCST as follows:

$$\frac{\partial N_{xx}}{\partial x} = 0 \quad (45)$$

$$\frac{\partial^2 M_{xx}}{\partial x^2} + \frac{\partial^2 P_1}{\partial x^2} + k_w w - k_p \frac{\partial^2 w}{\partial x^2} + q(x) = 0 \quad (46)$$

$$\frac{\partial^2 M_{nc}}{\partial x^2} + \frac{\partial^2 P_2}{\partial x^2} - \frac{1}{2} P_3 - Q = 0 \quad (47)$$

and the corresponding boundary conditions (BCs) at $x = 0$ and $x = L$, as:

$$N_{xx} = 0 \quad \text{or} \quad u = 0 \quad (48)$$

$$\frac{\partial M_{xx}}{\partial x} + \frac{\partial P_1}{\partial x} = 0 \quad \text{or} \quad w = 0 \quad (49)$$

$$M_{nc} + \frac{1}{2} P_2 = 0 \quad \text{or} \quad \gamma = 0 \quad (50)$$

$$M_{xx} + P_1 = 0 \quad \text{or} \quad \frac{\partial w}{\partial x} = 0 \quad (51)$$

The equilibrium equations of FG-CNTRC microbeam in terms of the displacements (u , w , and γ), are obtained by substituting Eqs. (33)–(39) into Eqs. (49)–(51), yielding:

$$A_{11} \frac{\partial^2 u}{\partial x^2} - B_{11} \frac{\partial^3 w}{\partial x^3} + E_{11} \frac{\partial^2 \gamma}{\partial x^2} = 0, \quad (52)$$

$$-B_{11} \frac{\partial^3 u}{\partial x^3} + (D_{11} + A_{13} l^2) \frac{\partial^4 w}{\partial x^4} - \left(F_{11} + \frac{1}{2} D_{11} l^2 \right) \frac{\partial^3 \gamma}{\partial x^3} - k_w w + k_p \frac{\partial^2 w}{\partial x^2} - q(x) = 0, \quad (53)$$

$$E_{11} \frac{\partial^2 u}{\partial x^2} - \left(F_{11} + \frac{1}{2} D_{13} l^2 \right) \frac{\partial^3 w}{\partial x^3} + \left(H_{11} + \frac{1}{4} B_{13} l^2 \right) \frac{\partial^2 \gamma}{\partial x^2} - \left(B_{13} + \frac{1}{4} E_{13} l^2 \right) \gamma = 0. \quad (54)$$

This analysis is carried out under several simplifying assumptions that may limit its practical accuracy. The FG-CNTRC microbeams are modeled as homogeneous continua with smoothly varying properties, thus neglecting microstructural defects and non-uniform CNT distribution. Linear elasticity and small deformations are assumed, so geometric and material nonlinearities under large loads are not considered. The adopted HoSDBTs use simplified kinematic assumptions, which may reduce accuracy for beams with extreme aspect ratios or highly graded materials. The supports are idealized as linear Winkler–Pasternak foundations with simply supported boundaries, which may not fully represent complex or nonlinear substrate behaviors. Finally, the MCST involves a single material length-scale parameter, omitting effects such as surface energy or microstructural interactions that could become important at very small scales.

5 Static Bending Analysis

The current study employed the Navier method using Fourier sine series to derive closed-form solution for the bending analysis of simply-supported FG-CNTRC microbeams. By integrating the MCST with higher-order shear deformation effects, the solution explicitly accounted for both nanoscale length-scale effects and transverse shear behavior. To begin with, the problem's boundary conditions were imposed. For simply-supported ends, the boundary equations are written as follows:

$$A_{11} \frac{\partial u}{\partial x} - B_{11} \frac{\partial^2 w}{\partial x^2} + E_{11} \frac{\partial \gamma}{\partial x} = 0 \quad (55)$$

$$w = 0 \quad (56)$$

$$E_{11} \frac{\partial u}{\partial x} - \left(F_{11} + \frac{1}{2} D_{13} l^2 \right) \frac{\partial^2 w}{\partial x^2} + \left(H_{11} + \frac{1}{4} B_{13} l^2 \right) \frac{\partial \gamma}{\partial x} = 0 \quad (57)$$

$$B_{11} \frac{\partial u}{\partial x} - \left(D_{11} + A_{13} l^2 \right) \frac{\partial^2 w}{\partial x^2} + \left(F_{11} + \frac{1}{2} D_{13} l^2 \right) \frac{\partial \gamma}{\partial x} = 0 \quad (58)$$

In formulation, the Navier method was used to derive closed-form solutions. This study started by representing the displacement fields as series of trigonometric functions multiplied by unknown coefficients. This form both satisfied the governing differential equations and inherently enforced the simply-supported boundary conditions at $x = 0$ and $x = L$, as shown below:

$$u(x) = \sum_{n=1}^N U_n \cos(\alpha_n x), \quad (59)$$

$$w(x) = \sum_{n=1}^N W_n \sin(\alpha_n x), \quad (60)$$

$$\gamma(x) = \sum_{n=1}^N \Psi_n \cos(\alpha_n x). \quad (61)$$

where, $\alpha_n = n\pi/L$ corresponds to the n -th half-wave, (U_n, W_n, Ψ_n) are the unknown modal amplitudes to be determined. The distributed load via a Fourier sine series was represented below [38]:

$$q(x) = \sum_{n=1}^N Q_n \sin(\alpha_n x) \quad (62)$$

where, each coefficient Q_n denotes the contribution of the n -th half-wave of the loading. Expanding the load in this way ensures perfect compatibility with the Navier series expansion of the displacement field. By matching loading $q(x)$ mode-by-mode with the assumed displacement form, this study could derive explicit expressions for deflection, internal bending moment, and the modal amplitudes (U_n, W_n, Ψ_n) in a straightforward and elegant manner. The coefficient Q_n is determined by exploiting the orthogonality of the sine functions [38]:

$$Q_n = \frac{2}{L} \int_0^L q(x) \sin(\alpha_n x) dx, \quad n = 1, 2, 3, \dots, N \quad (63)$$

Below are explicit expressions for three typical loading cases: uniform load, sinusoidal load, and point load [38]:
For uniformly distributed load: $q(x) = q_0$

$$Q_n = \begin{cases} \frac{4q_0}{n\pi}, & n \text{ odd} \\ 0, & n \text{ even.} \end{cases} \quad (64)$$

where, q_0 is the intensity of the uniformly distributed load.

For sinusoidal load: $q(x) = q_0 \sin\left(\frac{\pi x}{L}\right)$

Only the coefficient with $n = 1$ is non-zero:

$$Q_n = \begin{cases} q_0, & n = 1, \\ 0, & n \neq 1. \end{cases} \quad (65)$$

For point load: $q(x) = P\delta(x - x_p)$

$$Q_n = \frac{2P}{L} \sin(\alpha_n x_p), \quad n = 1, 2, 3, \dots \quad (66)$$

where, P denotes the magnitude of the point load, x_p is the location at which the point load is applied, and $\delta(\cdot)$ is the Dirac delta function. Substituting Eqs. (59)–(61) into Eqs. (52)–(54) yields the following system of algebraic equations:

$$\begin{bmatrix} K_{11} & K_{12} & K_{13} \\ K_{21} & K_{22} & K_{23} \\ K_{31} & K_{32} & K_{33} \end{bmatrix} \begin{bmatrix} U_n \\ W_n \\ \Psi_n \end{bmatrix} = \begin{bmatrix} 0 \\ Q_n \\ 0 \end{bmatrix} \quad (67)$$

where, the coefficients K_{ij} ($i, j = 1, 2, 3$) are given by:

$$\begin{aligned} K_{11} &= \alpha_n^2 A_{11}, K_{12} = K_{21} = -\alpha_n^3 B_{11}, K_{13} = K_{31} = \alpha_n^2 E_{11}, K_{22} = \alpha_n^4 (D_{11} + A_{13}l^2) + k_w + k_p \alpha_n^2, \\ K_{23} = K_{32} &= -\alpha_n^3 \left(F_{11} + \frac{1}{2} D_{13}l^2 \right), K_{33} = \alpha_n^2 \left(H_{11} + \frac{1}{4} B_{13}l^2 \right) + \left(B_{13} + \frac{1}{4} E_{13}l^2 \right) \end{aligned} \quad (68)$$

Solving Eq. (67), the modal amplitudes (U_n, W_n, Ψ_n) can be obtained as:

$$U_n = \frac{[-K_{12}K_{33} + K_{13}K_{32}] Q_n}{K_{11}(K_{22}K_{33} - K_{23}K_{32}) - K_{12}(K_{21}K_{33} - K_{23}K_{31}) + K_{13}(K_{21}K_{32} - K_{22}K_{31})} \quad (69)$$

$$W_n = \frac{[K_{11}K_{33} - K_{13}K_{31}] Q_n}{K_{11}(K_{22}K_{33} - K_{23}K_{32}) - K_{12}(K_{21}K_{33} - K_{23}K_{31}) + K_{13}(K_{21}K_{32} - K_{22}K_{31})} \quad (70)$$

$$\Psi_n = \frac{[K_{12}K_{31} - K_{11}K_{32}] Q_n}{K_{11}(K_{22}K_{33} - K_{23}K_{32}) - K_{12}(K_{21}K_{33} - K_{23}K_{31}) + K_{13}(K_{21}K_{32} - K_{22}K_{31})} \quad (71)$$

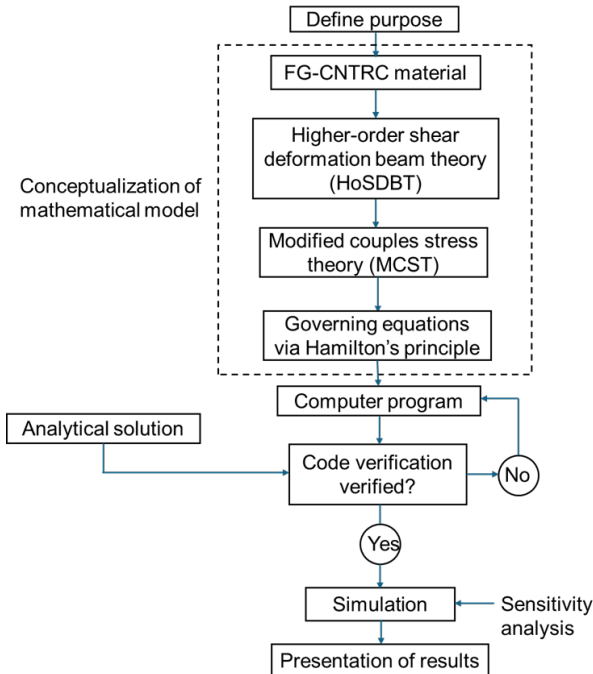


Figure 4. Flowchart of the analytical procedure

The analytical solution for static bending of FG-CNTRC microbeam can be obtained by substituting the expressions of the modal amplitudes (U_n , W_n , Ψ_n) obtained in Eqs. (69)–(71) into Eqs. (59)–(61).

Figure 4 presents a schematic flow diagram that outlines the overall methodological framework adopted in this study. It depicts the sequence of key stages beginning with the definition of the FG-CNTRC properties, followed by the formulation under the MCST and HoSDBTs, and culminating in the static bending analysis of FG-CNTRC microbeams.

6 Numerical Results and Discussion

This study conducted a comprehensive numerical investigation into the static bending, buckling, and free vibration behavior of simply supported FG-CNTRC microbeams with the previously obtained closed-form solutions. The microbeams were reinforced with CNTs embedded in a polymer matrix, with material properties characterized by the extended rule of mixtures. In this study, poly methyl methacrylate (PMMA) was used as the polymer matrix. The material properties of PMMA are given as follows [16, 17]: $E^m = 2.5\text{GPa}$, $\rho^m = 1190 \text{ kg/m}^3$, $v^m = 0.3$. The (10, 10) SWCNTs are considered as the reinforcement material, which have the material properties as [16, 17]: $E_{11}^{CNT} = 5646.6\text{GPa}$, $E_{22}^{CNT} = 7080\text{GPa}$, $G_{12}^{CNT} = 1944.5\text{GPa}$, $v_{12}^{CNT} = 0.175$, $\rho^{CNT} = 2100 \text{ kg/m}^3$. The CNT efficiency parameters (η_1 , η_2 , η_3) can be determined by matching the results from molecular dynamics [16, 17], as presented in Table 2.

Table 2. CNT efficiency parameters [16, 17]

CNT Efficiency Parameters	$V_{\text{CNT}}^* = 0.12$	$V_{\text{CNT}}^* = 0.17$	$V_{\text{CNT}}^* = 0.28$
η_1	0.137	0.142	0.141
η_2	1.022	1.626	1.585
η_3	0.715	1.138	1.109

In the context of the MCST, the material length-scale parameter l is not a universal constant but depends on the microstructure, geometry, and material composition of the system [44]. Experimental and theoretical studies have shown that l varies with structural dimensions (especially thickness or diameter) as well as inherent material features such as grain size or crystalline texture [44]. To enable a quantitative investigation of size effects in functionally graded microbeams, Simsek and Reddy [38] assumed a value for the material length-scale parameter, $l = 15\mu\text{m}$. The present work likewise treated $l = 15\mu\text{m}$ as a parameter (i.e., variable) to explore its influence on the size-dependent behavior of FG-CNTRC microbeams. Moreover, to clearly reflect the relative importance of size effects, this study normalized l by the microbeam thickness h , and presented results in terms of the nondimensional ratio h/l .

For convenience in analyzing the static bending behavior of FG-CNTRC microbeams, the following dimensionless parameters were defined:

Dimensionless transverse deflection:

$$\bar{w} = 100w \frac{E^m I}{q_0 L^4} \quad \text{for uniform and sinusoidal loads} \quad (72)$$

Dimensionless transverse deflection:

$$\bar{w} = 100w \frac{E^m I}{PL^3} \quad \text{for point loads} \quad (73)$$

where, $I = bh^3/12$ is the area moment of inertia of the microbeam's cross-section. Also, the dimensionless elastic constants of the elastic foundation were defined as:

$$K_w = \frac{k_w L^4}{E^m I}, K_p = \frac{k_p L^2}{E^m I} \quad (74)$$

6.1 Comparative Study

To validate the analytical solutions derived from using the MCST and HoSDBTs for simply-supported FG-CNTRC microbeams, a set of comparative studies was performed. In comparison, the static bending results in this study were benchmarked against those reported by Wattanasakulpong and Ungbhakorn [23]. The comparison is summarized in Table 3. The nondimensional deflection is defined as $\hat{w} = 100 \frac{E^m h^3}{q_0 L^4} w \left(\frac{L}{2}\right)$. The comparative results showed very close agreement, thus demonstrating high accuracy and consistency of the present analysis.

Table 3. Comparison of the dimensionless deflection, $\hat{w} = 100 \frac{E^m h^3}{q_0 L^4} w \left(\frac{L}{2}\right)$, of simply-supported UD beam

V_{CNT}^*	L/h	Uniform Load		Sinusoidal Load	
		Wattanasakulpong & Ungbhakorn [23]	Present	Wattanasakulpong & Ungbhakorn [23]	Present
0.12	10	0.704	0.740	0.562	0.569
	15	0.524	0.558	0.416	0.428
	20	0.461	0.495	0.365	0.378
0.17	10	0.449	0.472	0.358	0.360
	15	0.344	0.366	0.273	0.278
	20	0.307	0.328	0.243	0.249
0.28	10	0.325	0.339	0.26	0.262
	15	0.235	0.247	0.187	0.191
	20	0.203	0.215	0.161	0.166

6.2 Parametric Study

In this subsection, a numerical study was carried out to show how key design parameters affected the static bending behaviour of FG-CNTRC microbeams. The parameters analyzed included: material length scale parameter (h/l) from the MCST; CNT volume fraction (V_{CNT}^*); aspect ratio (L/h); elastic support via Winkler and Pasternak foundations (K_w and K_p), different beam models, and CNT gradation profiles of UD, FG-O, FG-X, and FG-V.

The maximum dimensionless deflections (\bar{w}) of FG-CNTRC microbeams were investigated across various beam models, the dimensionless material length scale parameter (h/l), aspect ratio (L/h), CNT volume fraction (V_{CNT}^*), and CNT distribution patterns of UD, FG-O, FG-X, and FG-V, as detailed in Table 4 to Table 9. The dimensionless maximum deflection (\bar{w}) for FG-CNTRC microbeams under a uniformly distributed load, first without an elastic foundation, then with one, is presented in Table 4 and Table 5, respectively. Table 6 and Table 7 show the dimensionless maximum deflection (\bar{w}) under a point load applied at the mid-span, for cases without and with an elastic foundation, respectively. Meanwhile, the dimensionless maximum deflection (\bar{w}) under a sinusoidal distributed load is reported for models without an elastic foundation in Table 8, and with an elastic foundation in Table 9. The results accord well with the expected trends: EBBT always yields the smallest deflection (underestimating bending) since it neglects shear deformation; FSDBT predicts the largest deflection, thus reflecting its first-order shear consideration and approximate shear correction. The higher-order theories (PSDBT, TSDBT, HSDBT, ESDBT, and ASDBT) cluster closely together, hence demonstrating their abilities to model shear deformation accurately with minimal inter-model discrepancy. This consistency confirms their capacity to represent shear profiles effectively without heavy dependence on correction factors. From Table 4 to Table 9, one can observe that significant differences among the beam theories (EBBT, FSDBT, and HoSDBTs) emerge when the slenderness ratio (L/h) is small (e.g., $L/h = 5$, i.e., for thick microbeams). As L/h increases (e.g., $L/h = 30$ or 50 , corresponding to slender microbeams), the predictions from all theories converge. In the thick-beam regime, reliance on EBBT or FSDBT may lead to substantial under- or over-estimation of deflection, so the use of HoSDBTs becomes essential for accuracy. Yet for slender microbeams, the simpler theories (EBBT or FSDBT) suffice and are computationally more efficient. The results clearly illustrated this convergence behavior, highlighting both the limitations of simpler models and the advantages of HoSDBTs; they provided strong methodological justification for selecting the appropriate theory based on the slenderness ratio (L/h).

The influence of the dimensionless material length scale parameter (h/l) on the static bending behavior of FG-CNTRC microbeams is evident in Table 4 to Table 9. In the MCST framework, the ratio h/l serves as the key indicator of size-dependent effects. When h/l is small (i.e., the internal length scale l is on the same order as the microbeam thickness h), couple-stress effects impart significant stiffening, thereby reducing the microbeam's deflection. In that regime, the intrinsic couple-stress contributions in the MCST markedly increase bending rigidity compared to the classical elasticity theory (CET). As h/l grows larger, the microstructural influence wanes and the MCST predictions smoothly converge to those of CET, to signify diminishing size effects. This behavior aligns with prior analytical and experimental investigations using the MCST-based beam models, which show that size effects are substantial at lower h/l values but become negligible once h/l exceeds roughly Table 4 to Table 9. Thus, the characteristic response, stiffer behavior at small h/l and a gradual return to classical behavior at large h/l , is a signature feature in micro- and nano-scale bending analyses under the MCST.

The numerical findings revealed a strong interplay between CNT volume fraction V_{CNT}^* and the distribution scheme. Raising the CNT volume fraction invariably stiffened the microbeam and lowered the maximum dimensionless deflection (\bar{w}), in agreement with prior studies showing reductions up to about 36% under comparable loading conditions. Moreover, the layout of reinforcement profoundly affected bending behavior: FG-X distributions

(with CNTs concentrated near the surfaces) yielded the smallest deflection, whereas FG-O layouts produced the largest, because the outer fiber reinforcement is the most effective in resisting bending stresses. The UD and FG-V patterns fell in between. Interestingly, as the CNT volume fraction V_{CNT}^* increased, the performance gap between different distribution strategies widened, indicating that optimizing stiffness demands careful selection of both volume fraction and gradient profile. These results underscored the vital influence of both CNT volume fraction and spatial gradation on the bending stiffness of FG-CNTRC microbeams. In particular, surface-rich configurations (e.g., FG-X) delivered superior stiffness and reduced deflection, in consistence with the literature [16, 23], whereas mid-plane-rich configurations (e.g., FG-O) led to higher deflections. As CNT loading increased, differences among distribution strategies became more pronounced. Therefore, for stiffness-targeted designs, a synergistic optimization of both CNT fraction and its distribution profile is strongly recommended.

Incorporating a Winkler–Pasternak elastic foundation markedly reduced the deflection of the microbeam across all CNT distribution schemes, though the degree of reduction depended on the material gradation. Microbeams with FG-X distributions (CNTs concentrated at the surfaces) gained the most from additional stiffening, resulting in the lowest deflection under foundation support. Meanwhile, FG-O microbeams also experienced significant deflection reduction on the order of 20 to 30%, yet remained the most flexible of the group, owing to the reinforcement concentrated near the mid-plane. The UD and FG-V distributions exhibited intermediate responses. These trends conformed to established mechanics of FG-CNT systems under elastic foundations, thus underscoring the compensatory effect that a foundation provided, especially for softer gradation profiles.

Changes in maximum dimensionless deflections (\bar{w}) of FG-CNTRC microbeams on an elastic foundation under uniform, point, and sinusoidal loads are depicted in Figure 5, Figure 6, and Figure 7, respectively. In these figures, the MCST-based higher-order shear deformation theories (FSDBT-MCST, and HoSDBTs-MCST) showed markedly lower deflections at $h/l \approx 1$, in some cases 40 to 50% below classical theory predictions. This underscored the capacity of the theory to capture microstructural stiffening effects that are significant at small scales. As h/l increased (i.e., the microbeam became “thicker” relative to the material length scale), the influence of the intrinsic length scale parameter waned, and the MCST results gradually converged toward classical (shear deformation) curves. This behavior suggests that for thicker beams, classical shear deformation theories become sufficiently accurate.

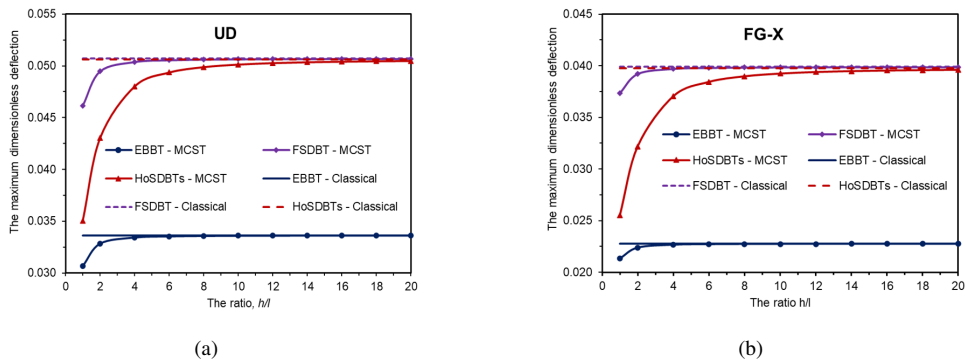


Figure 5. Maximum dimensionless deflections (\bar{w}) of FG-CNTRC microbeams resting on elastic foundation under uniform load ($L/h = 15$, $V_{CNT}^* = 0.12$, $K_w = 10$, $K_p = 5$)

Figure 8 illustrates how the maximum dimensionless deflection (\bar{w}) of FG-CNTRC microbeams on an elastic foundation varies with the slenderness ratio (L/h). Four CNT distribution schemes, UD, FG-O, FG-X, and FG-V, are included in this depiction. It is evident that deflections differ markedly at low L/h values but tend to converge toward stable levels as L/h increases. Among the four distribution types, FG-O exhibited the greatest deflection, followed by FG-V, UD, and FG-X.

The impact of the CNT volume fraction V_{CNT}^* on the static bending behavior of FG-CNTRC microbeams is illustrated in Figure 9. The uniform, sinusoidal, and point loads were considered in this investigation. The input data was considered as $h = 2l$, $K_w = 10$ and $K_p = 5$. It can be observed that an increase in the CNT volume fraction V_{CNT}^* in the FG-CNTRC microbeams led to higher composite stiffness; under a given static bending load, the maximum deflection decreased. However, the extent of deflection reduction might diminish at larger values of V_{CNT}^* as the gain in stiffness became marginal.

Figure 10 depicts how the maximum dimensionless deflection (\bar{w}) of FG-CNTRC microbeams on an elastic foundation varies along the normalized beam axis (x/L) under uniform, point, and sinusoidal loads. The deflection profiles are symmetric about the mid-axis ($x/L = 0.5$) for all CNT distribution schemes. Once again, the influence of CNT distribution is clear the ranking of maximum deflections is FG-O > FG-V > UD > FG-X.

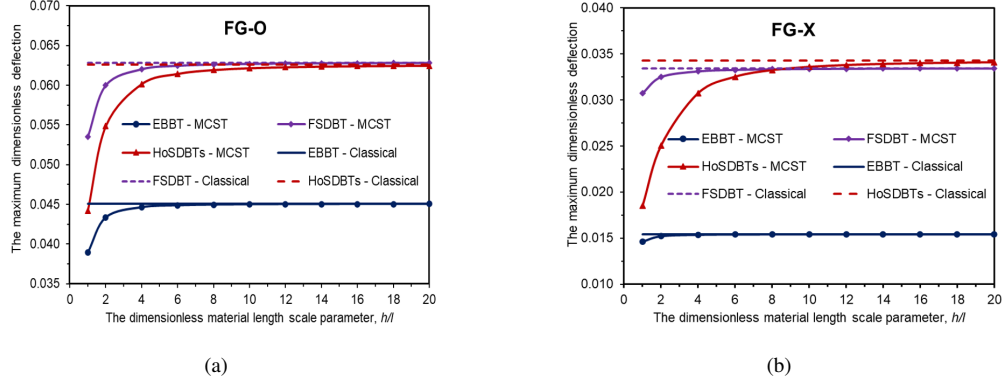


Figure 6. Maximum dimensionless deflections (\bar{w}) of FG-CNTRC microbeams resting on elastic foundation under point load ($L/h = 15, V_{CNT}^* = 0.28, K_w = 10, K_p = 5, x_P = 0.5L$)

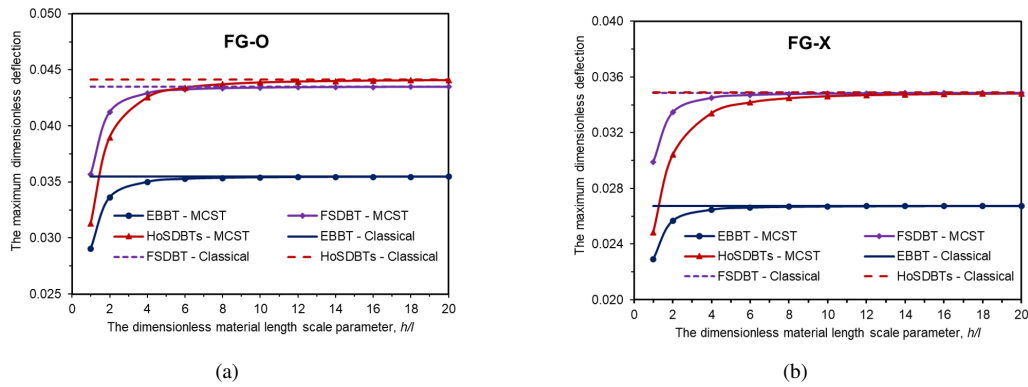


Figure 7. Maximum dimensionless deflections (\bar{w}) of FG-CNTRC microbeams resting on elastic foundation under sinusoidal load ($L/h = 15, V_{CNT}^* = 0.17, K_w = 10, K_p = 5$)

Table 4. Maximum dimensionless deflection (\bar{w}) of FG-CNTRC microbeams under uniform load ($V_{CNT}^* = 0.12$ and without elastic foundation)

h/l	Model	L/h=5				L/h=10				L/h=50			
		UD	FG-O	FG-X	FG-V	UD	FG-O	FG-X	FG-V	UD	FG-O	FG-X	FG-V
1	EBBT	0.0311	0.0557	0.0216	0.0436	0.0311	0.0557	0.0216	0.0436	0.0311	0.0557	0.0216	0.0436
	FSDBT	0.1668	0.1815	0.1599	0.1737	0.0352	0.0594	0.0257	0.0474	0.0326	0.0571	0.0231	0.0449
	PSDBT	0.0701	0.0981	0.0581	0.0805	0.0322	0.0569	0.0226	0.0446	0.0315	0.0562	0.0219	0.0439
	TSDBT	0.0702	0.0984	0.0584	0.0806	0.0323	0.0570	0.0226	0.0446	0.0315	0.0562	0.0220	0.0439
	HSDBT	0.0700	0.0980	0.0581	0.0805	0.0322	0.0569	0.0226	0.0446	0.0315	0.0562	0.0219	0.0439
	ESDBT	0.0694	0.0979	0.0578	0.0799	0.0322	0.0569	0.0226	0.0446	0.0315	0.0562	0.0219	0.0439
	ASDBT	0.0694	0.0979	0.0578	0.0799	0.0322	0.0569	0.0226	0.0446	0.0315	0.0562	0.0219	0.0439
2	EBBT	0.0333	0.0634	0.0226	0.0481	0.0333	0.0634	0.0226	0.0481	0.0333	0.0634	0.0226	0.0481
	FSDBT	0.1865	0.2123	0.1760	0.1987	0.0377	0.0676	0.0270	0.0524	0.0349	0.0649	0.0242	0.0496
	PSDBT	0.1243	0.1664	0.1088	0.1374	0.0360	0.0664	0.0252	0.0507	0.0343	0.0645	0.0235	0.0490
	TSDBT	0.1239	0.1672	0.1085	0.1370	0.0360	0.0664	0.0252	0.0507	0.0343	0.0645	0.0235	0.0490
	HSDBT	0.1243	0.1663	0.1088	0.1373	0.0360	0.0663	0.0252	0.0507	0.0343	0.0645	0.0235	0.0490
	ESDBT	0.1223	0.1666	0.1071	0.1355	0.0360	0.0664	0.0251	0.0507	0.0343	0.0645	0.0235	0.0490
	ASDBT	0.1223	0.1666	0.1071	0.1355	0.0360	0.0664	0.0251	0.0507	0.0343	0.0645	0.0235	0.0490
4	EBBT	0.0340	0.0656	0.0229	0.0494	0.0340	0.0656	0.0229	0.0494	0.0340	0.0656	0.0229	0.0494
	FSDBT	0.1922	0.2220	0.1805	0.2062	0.0384	0.0700	0.0273	0.0538	0.0356	0.0672	0.0245	0.0510
	PSDBT	0.1648	0.2141	0.1494	0.1793	0.0378	0.0699	0.0266	0.0532	0.0353	0.0672	0.0242	0.0508
	TSDBT	0.1635	0.2151	0.1479	0.1781	0.0378	0.0699	0.0266	0.0532	0.0353	0.0672	0.0242	0.0508

h/l	Model	L/h=5				L/h=10				L/h=50			
		UD	FG-O	FG-X	FG-V	UD	FG-O	FG-X	FG-V	UD	FG-O	FG-X	FG-V
	HSDBT	0.1649	0.2140	0.1495	0.1794	0.0378	0.0699	0.0266	0.0532	0.0353	0.0672	0.0242	0.0508
	ESDBT	0.1613	0.2150	0.1455	0.1759	0.0377	0.0699	0.0266	0.0532	0.0353	0.0672	0.0242	0.0508
	ASDBT	0.1613	0.2150	0.1455	0.1759	0.0377	0.0699	0.0266	0.0532	0.0353	0.0672	0.0242	0.0508
8	EBBT	0.0341	0.0662	0.0230	0.0497	0.0341	0.0662	0.0230	0.0497	0.0341	0.0662	0.0230	0.0497
	FSDBT	0.1937	0.2246	0.1816	0.2082	0.0386	0.0706	0.0274	0.0541	0.0357	0.0678	0.0246	0.0513
	PSDBT	0.1807	0.2322	0.1659	0.1957	0.0384	0.0709	0.0272	0.0540	0.0357	0.0679	0.0245	0.0513
	TSDBT	0.1789	0.2332	0.1637	0.1941	0.0384	0.0710	0.0272	0.0540	0.0357	0.0679	0.0245	0.0513
	HSDBT	0.1808	0.2321	0.1661	0.1958	0.0384	0.0709	0.0272	0.0540	0.0357	0.0679	0.0245	0.0513
	ESDBT	0.1765	0.2334	0.1608	0.1916	0.0384	0.0710	0.0271	0.0540	0.0356	0.0680	0.0245	0.0513
	ASDBT	0.1765	0.2334	0.1608	0.1916	0.0384	0.0710	0.0271	0.0540	0.0356	0.0680	0.0245	0.0513
10	EBBT	0.0341	0.0663	0.0230	0.0498	0.0341	0.0663	0.0230	0.0498	0.0341	0.0663	0.0230	0.0498
	FSDBT	0.1939	0.2249	0.1818	0.2084	0.0386	0.0707	0.0274	0.0542	0.0357	0.0679	0.0246	0.0514
	PSDBT	0.1828	0.2347	0.1682	0.1979	0.0385	0.0711	0.0273	0.0541	0.0357	0.0680	0.0245	0.0513
	TSDBT	0.1810	0.2356	0.1659	0.1962	0.0385	0.0711	0.0272	0.0541	0.0357	0.0680	0.0245	0.0513
	HSDBT	0.1829	0.2345	0.1683	0.1981	0.0385	0.0711	0.0273	0.0541	0.0357	0.0680	0.0245	0.0513
	ESDBT	0.1785	0.2359	0.1629	0.1937	0.0384	0.0712	0.0272	0.0541	0.0357	0.0681	0.0245	0.0513
	ASDBT	0.1785	0.2359	0.1629	0.1937	0.0384	0.0712	0.0272	0.0541	0.0357	0.0681	0.0245	0.0513
CET	EBBT	0.0342	0.0664	0.0230	0.0498	0.0342	0.0664	0.0230	0.0498	0.0342	0.0664	0.0230	0.0498
	FSDBT	0.1942	0.2254	0.1820	0.2089	0.0386	0.0708	0.0274	0.0543	0.0358	0.0680	0.0246	0.0514
	PSDBT	0.1868	0.2391	0.1724	0.2021	0.0386	0.0713	0.0274	0.0543	0.0358	0.0682	0.0246	0.0514
	TSDBT	0.1849	0.2401	0.1699	0.2002	0.0386	0.0714	0.0274	0.0543	0.0358	0.0682	0.0246	0.0514
	HSDBT	0.1869	0.2390	0.1725	0.2022	0.0386	0.0713	0.0274	0.0543	0.0358	0.0682	0.0246	0.0514
	ESDBT	0.1823	0.2404	0.1668	0.1977	0.0386	0.0714	0.0273	0.0542	0.0358	0.0682	0.0246	0.0514
	ASDBT	0.1823	0.2404	0.1668	0.1977	0.0386	0.0714	0.0273	0.0542	0.0358	0.0682	0.0246	0.0514

Table 5. Maximum dimensionless deflection (\bar{w}) of FG-CNTRC microbeams under uniform load (V_{CNT}^* and with elastic foundation $K_w = 10$, $K_p = 5$)

h/l	Model	L/h=10				L/h=20				L/h=50			
		UD	FG-O	FG-X	FG-V	UD	FG-O	FG-X	FG-V	UD	FG-O	FG-X	FG-V
1	EBBT	0.0307	0.0543	0.0213	0.0427	0.0307	0.0543	0.0213	0.0427	0.0307	0.0543	0.0213	0.0427
	FSDBT	0.1544	0.1670	0.1485	0.1604	0.0346	0.0578	0.0254	0.0464	0.0321	0.0556	0.0228	0.0440
	PSDBT	0.0678	0.0937	0.0566	0.0775	0.0318	0.0555	0.0224	0.0437	0.0311	0.0547	0.0217	0.0431
	TSDBT	0.0679	0.0940	0.0568	0.0776	0.0318	0.0555	0.0224	0.0437	0.0311	0.0547	0.0217	0.0431
	HSDBT	0.0678	0.0937	0.0565	0.0775	0.0318	0.0555	0.0224	0.0437	0.0311	0.0547	0.0217	0.0431
	ESDBT	0.0672	0.0935	0.0563	0.0770	0.0318	0.0555	0.0224	0.0437	0.0311	0.0547	0.0217	0.0430
	ASDBT	0.0672	0.0935	0.0563	0.0770	0.0318	0.0555	0.0224	0.0437	0.0311	0.0547	0.0217	0.0430
2	EBBT	0.0328	0.0615	0.0224	0.0470	0.0328	0.0615	0.0224	0.0470	0.0328	0.0615	0.0224	0.0470
	FSDBT	0.1711	0.1927	0.1622	0.1814	0.0370	0.0655	0.0266	0.0511	0.0343	0.0630	0.0239	0.0485
	PSDBT	0.1173	0.1541	0.1034	0.1289	0.0354	0.0643	0.0249	0.0495	0.0338	0.0626	0.0233	0.0479
	TSDBT	0.1169	0.1548	0.1032	0.1286	0.0354	0.0644	0.0249	0.0495	0.0338	0.0626	0.0233	0.0479
	HSDBT	0.1173	0.1540	0.1034	0.1289	0.0354	0.0643	0.0249	0.0495	0.0338	0.0626	0.0233	0.0479
	ESDBT	0.1155	0.1543	0.1018	0.1272	0.0354	0.0644	0.0248	0.0495	0.0338	0.0626	0.0233	0.0479
	ASDBT	0.1155	0.1543	0.1018	0.1272	0.0354	0.0644	0.0248	0.0495	0.0338	0.0626	0.0233	0.0479
4	EBBT	0.0334	0.0637	0.0227	0.0483	0.0334	0.0637	0.0227	0.0483	0.0334	0.0637	0.0227	0.0483
	FSDBT	0.1759	0.2006	0.1660	0.1876	0.0377	0.0678	0.0270	0.0524	0.0350	0.0652	0.0242	0.0498
	PSDBT	0.1527	0.1942	0.1394	0.1651	0.0371	0.0676	0.0263	0.0519	0.0348	0.0651	0.0240	0.0496
	TSDBT	0.1516	0.1949	0.1381	0.1381	0.0371	0.0677	0.0263	0.0519	0.0348	0.0651	0.0240	0.0496
	HSDBT	0.1528	0.1941	0.1395	0.1652	0.0371	0.0676	0.0263	0.0519	0.0348	0.0651	0.0240	0.0496
	ESDBT	0.1497	0.1949	0.1360	0.1623	0.0371	0.0677	0.0263	0.0519	0.0347	0.0651	0.0240	0.0496
	ASDBT	0.1497	0.1949	0.1360	0.1623	0.0371	0.0677	0.0263	0.0519	0.0347	0.0651	0.0240	0.0496
8	EBBT	0.0336	0.0642	0.0227	0.0486	0.0336	0.0642	0.0227	0.0486	0.0336	0.0642	0.0227	0.0486
	FSDBT	0.1771	0.2027	0.1670	0.1892	0.0379	0.0684	0.0270	0.0528	0.0351	0.0657	0.0243	0.0501

h/l	Model	L/h=10				L/h=20				L/h=50			
		UD	FG-O	FG-X	FG-V	UD	FG-O	FG-X	FG-V	UD	FG-O	FG-X	FG-V
	PSDBT	0.1662	0.2089	0.1537	0.1789	0.0377	0.0686	0.0268	0.0526	0.0351	0.0658	0.0242	0.0501
	TSDBT	0.1648	0.2097	0.1518	0.1776	0.0377	0.0687	0.0268	0.0526	0.0351	0.0658	0.0242	0.0501
	HSDBT	0.1663	0.2088	0.1538	0.1790	0.0377	0.0686	0.0268	0.0526	0.0351	0.0658	0.0242	0.0501
	ESDBT	0.1627	0.2099	0.1493	0.1755	0.0377	0.0687	0.0268	0.0526	0.0351	0.0659	0.0242	0.0500
	ASDBT	0.1627	0.2099	0.1493	0.1755	0.0377	0.0687	0.0268	0.0526	0.0351	0.0659	0.0242	0.0500
10	EBBT	0.0336	0.0643	0.0227	0.0486	0.0336	0.0643	0.0227	0.0486	0.0336	0.0643	0.0227	0.0486
	FSDBT	0.1773	0.2029	0.1671	0.1894	0.0379	0.0684	0.0270	0.0528	0.0351	0.0658	0.0243	0.0501
	PSDBT	0.1681	0.2109	0.1556	0.1808	0.0378	0.0688	0.0269	0.0527	0.0351	0.0659	0.0242	0.0501
	TSDBT	0.1666	0.2117	0.1537	0.1794	0.0378	0.0688	0.0269	0.0527	0.0351	0.0659	0.0242	0.0501
	HSDBT	0.1682	0.2108	0.1557	0.1809	0.0378	0.0688	0.0269	0.0527	0.0351	0.0659	0.0242	0.0501
	ESDBT	0.1644	0.2119	0.1511	0.1773	0.0377	0.0689	0.0269	0.0527	0.0351	0.0659	0.0242	0.0501
	ASDBT	0.1644	0.2119	0.1511	0.1773	0.0377	0.0689	0.0269	0.0527	0.0351	0.0659	0.0242	0.0501
CET	EBBT	0.0336	0.0644	0.0228	0.0487	0.0336	0.0644	0.0228	0.0487	0.0336	0.0644	0.0228	0.0487
	FSDBT	0.1775	0.2034	0.1673	0.1898	0.0379	0.0686	0.0271	0.0529	0.0352	0.0659	0.0243	0.0502
	PSDBT	0.1714	0.2145	0.1592	0.1842	0.0379	0.0690	0.0270	0.0529	0.0352	0.0661	0.0243	0.0502
	TSDBT	0.1698	0.2153	0.1571	0.1827	0.0379	0.0691	0.0270	0.0529	0.0352	0.0661	0.0243	0.0502
	HSDBT	0.1715	0.2144	0.1593	0.1843	0.0379	0.0690	0.0270	0.0529	0.0352	0.0661	0.0243	0.0502
	ESDBT	0.1677	0.2155	0.1545	0.1806	0.0379	0.0691	0.0270	0.0529	0.0352	0.0661	0.0243	0.0502
	ASDBT	0.1677	0.2155	0.1545	0.1806	0.0379	0.0691	0.0270	0.0529	0.0352	0.0661	0.0243	0.0502

Table 6. Maximum dimensionless deflection (\bar{w}) of FG-CNTRC microbeams under uniform load ($V_{CNT}^* = 0.17$ and without elastic foundation)

h/l	Model	L/h=5				L/h=30				L/h=50			
		UD	FG-O	FG-X	FG-V	UD	FG-O	FG-X	FG-V	UD	FG-O	FG-X	FG-V
1	EBBT	0.0215	0.0394	0.0147	0.0306	0.0215	0.0394	0.0147	0.0306	0.0215	0.0394	0.0147	0.0306
	FSDBT	0.1524	0.1562	0.1409	0.1507	0.0258	0.0432	0.0189	0.0346	0.0231	0.0408	0.0162	0.0320
	PSDBT	0.0596	0.0826	0.0461	0.0644	0.0227	0.0408	0.0157	0.0317	0.0219	0.0399	0.0151	0.0310
	TSDBT	0.0594	0.0822	0.0469	0.0646	0.0227	0.0408	0.0157	0.0317	0.0219	0.0399	0.0151	0.0310
	HSDBT	0.0595	0.0826	0.0460	0.0644	0.0227	0.0408	0.0157	0.0317	0.0219	0.0399	0.0151	0.0310
	ESDBT	0.0586	0.0810	0.0470	0.0640	0.0227	0.0407	0.0158	0.0317	0.0219	0.0399	0.0151	0.0310
	ASDBT	0.0586	0.0810	0.0470	0.0640	0.0227	0.0407	0.0158	0.0317	0.0219	0.0399	0.0151	0.0310
2	EBBT	0.0227	0.0439	0.0153	0.0332	0.0227	0.0439	0.0153	0.0332	0.0227	0.0439	0.0153	0.0332
	FSDBT	0.1766	0.1870	0.1618	0.1776	0.0274	0.0482	0.0197	0.0376	0.0244	0.0455	0.0169	0.0348
	PSDBT	0.1095	0.1400	0.0934	0.1149	0.0255	0.0469	0.0179	0.0359	0.0237	0.0450	0.0162	0.0342
	TSDBT	0.1084	0.1391	0.0938	0.1143	0.0255	0.0469	0.0179	0.0359	0.0237	0.0450	0.0162	0.0342
	HSDBT	0.1096	0.1400	0.0933	0.1149	0.0255	0.0469	0.0178	0.0359	0.0237	0.0450	0.0162	0.0342
	ESDBT	0.1062	0.1372	0.0931	0.1126	0.0255	0.0469	0.0179	0.0359	0.0237	0.0450	0.0162	0.0342
	ASDBT	0.1062	0.1372	0.0931	0.1126	0.0255	0.0469	0.0179	0.0359	0.0237	0.0450	0.0162	0.0342
4	EBBT	0.0230	0.0452	0.0154	0.0340	0.0230	0.0452	0.0154	0.0340	0.0230	0.0452	0.0154	0.0340
	FSDBT	0.1876	0.2003	0.1716	0.1895	0.0278	0.0497	0.0200	0.0385	0.0247	0.0468	0.0171	0.0356
	PSDBT	0.1469	0.1775	0.1362	0.1537	0.0271	0.0493	0.0195	0.0379	0.0245	0.0467	0.0169	0.0354
	TSDBT	0.1444	0.1761	0.1347	0.1517	0.0270	0.0493	0.0195	0.0379	0.0245	0.0467	0.0169	0.0354
	HSDBT	0.1471	0.1776	0.1363	0.1539	0.0271	0.0493	0.0195	0.0379	0.0245	0.0467	0.0169	0.0354
	ESDBT	0.1411	0.1740	0.1323	0.1488	0.0270	0.0493	0.0195	0.0379	0.0245	0.0467	0.0169	0.0354
	ASDBT	0.1411	0.1740	0.1323	0.1488	0.0270	0.0493	0.0195	0.0379	0.0245	0.0467	0.0169	0.0354
8	EBBT	0.0231	0.0455	0.0155	0.0342	0.0231	0.0455	0.0155	0.0342	0.0231	0.0455	0.0155	0.0342
	FSDBT	0.1926	0.2059	0.1761	0.1946	0.0279	0.0501	0.0200	0.0387	0.0248	0.0472	0.0171	0.0358
	PSDBT	0.1615	0.1913	0.1550	0.1693	0.0276	0.0500	0.0202	0.0386	0.0247	0.0471	0.0172	0.0358
	TSDBT	0.1583	0.1896	0.1523	0.1665	0.0276	0.0500	0.0202	0.0386	0.0247	0.0472	0.0172	0.0358
	HSDBT	0.1617	0.1914	0.1552	0.1695	0.0276	0.0500	0.0201	0.0386	0.0247	0.0471	0.0172	0.0358
	ESDBT	0.1545	0.1874	0.1489	0.1630	0.0276	0.0500	0.0202	0.0385	0.0247	0.0472	0.0172	0.0358
	ASDBT	0.1545	0.1874	0.1489	0.1630	0.0276	0.0500	0.0202	0.0385	0.0247	0.0472	0.0172	0.0358

<i>h/l</i>	Model	L/h=5				L/h=30				L/h=50			
		UD	FG-O	FG-X	FG-V	UD	FG-O	FG-X	FG-V	UD	FG-O	FG-X	FG-V
10	EBBT	0.0231	0.0456	0.0155	0.0342	0.0231	0.0456	0.0155	0.0342	0.0231	0.0456	0.0155	0.0342
	FSDBT	0.1935	0.2069	0.1770	0.1956	0.0279	0.0501	0.0200	0.0388	0.0248	0.0472	0.0171	0.0358
	PSDBT	0.1634	0.1931	0.1576	0.1714	0.0277	0.0501	0.0202	0.0387	0.0248	0.0472	0.0172	0.0358
	TSDBT	0.1601	0.1914	0.1547	0.1685	0.0277	0.0501	0.0203	0.0387	0.0248	0.0472	0.0172	0.0358
	HSDBT	0.1637	0.1932	0.1578	0.1716	0.0277	0.0501	0.0202	0.0387	0.0248	0.0472	0.0172	0.0358
	ESDBT	0.1563	0.1892	0.1512	0.1650	0.0276	0.0501	0.0202	0.0386	0.0248	0.0472	0.0172	0.0358
	ASDBT	0.1563	0.1892	0.1512	0.1650	0.0276	0.0501	0.0202	0.0386	0.0248	0.0472	0.0172	0.0358
CET	EBBT	0.0231	0.0457	0.0155	0.0342	0.0231	0.0457	0.0155	0.0342	0.0231	0.0457	0.0155	0.0342
	FSDBT	0.1964	0.2099	0.1797	0.1985	0.0279	0.0502	0.0200	0.0388	0.0249	0.0473	0.0171	0.0359
	PSDBT	0.1671	0.1965	0.1626	0.1753	0.0278	0.0502	0.0204	0.0388	0.0248	0.0473	0.0173	0.0359
	TSDBT	0.1636	0.1947	0.1593	0.1722	0.0278	0.0502	0.0204	0.0388	0.0248	0.0473	0.0173	0.0359
	HSDBT	0.1674	0.1966	0.1628	0.1756	0.0278	0.0502	0.0204	0.0388	0.0248	0.0473	0.0173	0.0359
	ESDBT	0.1596	0.1925	0.1555	0.1685	0.0278	0.0502	0.0204	0.0388	0.0248	0.0473	0.0173	0.0359
	ASDBT	0.1596	0.1925	0.1555	0.1685	0.0278	0.0502	0.0204	0.0388	0.0248	0.0473	0.0173	0.0359

Table 7. Maximum dimensionless deflection (\bar{w}) of FG-CNTRC microbeams under point load ($V_{CNT}^* = 0.28$ and with elastic foundation $K_w = 10, K_p = 5$)

<i>h/l</i>	Model	L/h=5				L/h=30				L/h=50			
		UD	FG-O	FG-X	FG-V	UD	FG-O	FG-X	FG-V	UD	FG-O	FG-X	FG-V
1	EBBT	0.0214	0.0389	0.0146	0.0303	0.0214	0.0389	0.0146	0.0303	0.0214	0.0389	0.0146	0.0303
	FSDBT	0.1465	0.1500	0.1359	0.1450	0.0257	0.0427	0.0188	0.0342	0.0229	0.0403	0.0162	0.0317
	PSDBT	0.0586	0.0808	0.0455	0.0633	0.0226	0.0403	0.0156	0.0314	0.0218	0.0394	0.0150	0.0307
	TSDBT	0.0585	0.0804	0.0463	0.0635	0.0226	0.0403	0.0157	0.0314	0.0218	0.0394	0.0150	0.0307
	HSDBT	0.0586	0.0808	0.0454	0.0633	0.0226	0.0403	0.0156	0.0314	0.0218	0.0394	0.0150	0.0307
	ESDBT	0.0577	0.0792	0.0464	0.0629	0.0226	0.0403	0.0157	0.0314	0.0218	0.0394	0.0150	0.0307
	ASDBT	0.0577	0.0792	0.0464	0.0629	0.0226	0.0403	0.0157	0.0314	0.0218	0.0394	0.0150	0.0307
2	EBBT	0.0225	0.0434	0.0152	0.0329	0.0225	0.0434	0.0152	0.0329	0.0225	0.0434	0.0152	0.0329
	FSDBT	0.1691	0.1785	0.1555	0.1700	0.0272	0.0476	0.0196	0.0372	0.0242	0.0449	0.0168	0.0345
	PSDBT	0.1065	0.1351	0.0912	0.1115	0.0253	0.0463	0.0178	0.0355	0.0236	0.0444	0.0161	0.0339
	TSDBT	0.1054	0.1342	0.0915	0.1109	0.0253	0.0463	0.0178	0.0356	0.0236	0.0444	0.0162	0.0339
	HSDBT	0.1065	0.1351	0.0911	0.1115	0.0253	0.0463	0.0178	0.0355	0.0236	0.0444	0.0161	0.0339
	ESDBT	0.1033	0.1324	0.0908	0.1093	0.0253	0.0463	0.0178	0.0355	0.0236	0.0444	0.0162	0.0339
	ASDBT	0.1033	0.1324	0.0908	0.1093	0.0253	0.0463	0.0178	0.0355	0.0236	0.0444	0.0162	0.0339
4	EBBT	0.0229	0.0446	0.0154	0.0337	0.0229	0.0446	0.0154	0.0337	0.0229	0.0446	0.0154	0.0337
	FSDBT	0.1794	0.1909	0.1647	0.1811	0.0276	0.0490	0.0198	0.0381	0.0246	0.0462	0.0170	0.0353
	PSDBT	0.1415	0.1698	0.1315	0.1478	0.0269	0.0486	0.0194	0.0375	0.0243	0.0461	0.0168	0.0351
	TSDBT	0.1391	0.1685	0.1301	0.1458	0.0268	0.0486	0.0194	0.0375	0.0243	0.0461	0.0168	0.0351
	HSDBT	0.1416	0.1698	0.1315	0.1479	0.0269	0.0486	0.0194	0.0375	0.0243	0.0461	0.0168	0.0351
	ESDBT	0.1360	0.1665	0.1278	0.1431	0.0268	0.0486	0.0194	0.0375	0.0243	0.0461	0.0168	0.0350
	ASDBT	0.1360	0.1665	0.1278	0.1431	0.0268	0.0486	0.0194	0.0375	0.0243	0.0461	0.0168	0.0350
8	EBBT	0.0229	0.0449	0.0154	0.0338	0.0229	0.0449	0.0154	0.0338	0.0229	0.0449	0.0154	0.0338
	FSDBT	0.1841	0.1961	0.1690	0.1859	0.0277	0.0494	0.0199	0.0383	0.0247	0.0466	0.0170	0.0355
	PSDBT	0.1549	0.1824	0.1489	0.1621	0.0274	0.0493	0.0200	0.0382	0.0246	0.0465	0.0171	0.0354
	TSDBT	0.1519	0.1808	0.1464	0.1594	0.0274	0.0493	0.0201	0.0382	0.0246	0.0465	0.0171	0.0354
	HSDBT	0.1552	0.1825	0.1491	0.1623	0.0274	0.0493	0.0200	0.0382	0.0246	0.0465	0.0171	0.0354
	ESDBT	0.1484	0.1788	0.1432	0.1562	0.0273	0.0493	0.0200	0.0381	0.0246	0.0465	0.0171	0.0354
	ASDBT	0.1484	0.1788	0.1432	0.1562	0.0273	0.0493	0.0200	0.0381	0.0246	0.0465	0.0171	0.0354
10	EBBT	0.0230	0.0450	0.0154	0.0339	0.0230	0.0450	0.0154	0.0339	0.0230	0.0450	0.0154	0.0339
	FSDBT	0.1850	0.1970	0.1698	0.1868	0.0277	0.0494	0.0199	0.0383	0.0247	0.0466	0.0170	0.0355
	PSDBT	0.1567	0.1840	0.1513	0.1640	0.0275	0.0494	0.0201	0.0383	0.0246	0.0466	0.0171	0.0355
	TSDBT	0.1537	0.1825	0.1486	0.1613	0.0275	0.0494	0.0201	0.0382	0.0246	0.0466	0.0171	0.0355
	HSDBT	0.1570	0.1841	0.1515	0.1642	0.0275	0.0494	0.0201	0.0383	0.0246	0.0466	0.0171	0.0355

<i>h/l</i>	Model	L/h=5				L/h=30				L/h=50			
		UD	FG-O	FG-X	FG-V	UD	FG-O	FG-X	FG-V	UD	FG-O	FG-X	FG-V
	ESDBT	0.1500	0.1804	0.1453	0.1580	0.0274	0.0494	0.0201	0.0382	0.0246	0.0466	0.0171	0.0355
	ASDBT	0.1500	0.1804	0.1453	0.1580	0.0274	0.0494	0.0201	0.0382	0.0246	0.0466	0.0171	0.0355
CET	EBBT	0.0230	0.0451	0.0154	0.0339	0.0230	0.0451	0.0154	0.0339	0.0230	0.0451	0.0154	0.0339
	FSDBT	0.1877	0.1998	0.1724	0.1895	0.0277	0.0495	0.0199	0.0384	0.0247	0.0467	0.0170	0.0355
	PSDBT	0.1601	0.1871	0.1559	0.1676	0.0276	0.0495	0.0203	0.0384	0.0247	0.0467	0.0172	0.0356
	TSDBT	0.1568	0.1855	0.1529	0.1647	0.0276	0.0495	0.0203	0.0384	0.0247	0.0467	0.0172	0.0355
	HSDBT	0.1604	0.1872	0.1561	0.1679	0.0276	0.0495	0.0203	0.0384	0.0247	0.0467	0.0172	0.0356
	ESDBT	0.1531	0.1834	0.1493	0.1613	0.0276	0.0495	0.0203	0.0384	0.0246	0.0467	0.0172	0.0355
	ASDBT	0.1531	0.1834	0.1493	0.1613	0.0276	0.0495	0.0203	0.0384	0.0246	0.0467	0.0172	0.0355

Table 8. Maximum dimensionless deflection (\bar{w}) of FG-CNTRC microbeams under sinusoidal load ($V_{CNT}^* = 0.17$ and without elastic foundation)

<i>h/l</i>	Model	L/h=5				L/h=30				L/h=50			
		UD	FG-O	FG-X	FG-V	UD	FG-O	FG-X	FG-V	UD	FG-O	FG-X	FG-V
1	EBBT	0.0166	0.0295	0.0115	0.0232	0.0166	0.0295	0.0115	0.0232	0.0166	0.0295	0.0115	0.0232
	FSDBT	0.0803	0.0875	0.0761	0.0835	0.0185	0.0313	0.0135	0.0250	0.0173	0.0302	0.0122	0.0239
	PSDBT	0.0349	0.0494	0.0283	0.0403	0.0171	0.0301	0.0120	0.0237	0.0168	0.0298	0.0117	0.0234
	TSDBT	0.0350	0.0495	0.0285	0.0403	0.0171	0.0301	0.0120	0.0237	0.0168	0.0298	0.0117	0.0234
	HSDBT	0.0349	0.0494	0.0283	0.0402	0.0171	0.0301	0.0120	0.0237	0.0168	0.0298	0.0117	0.0234
	ESDBT	0.0346	0.0492	0.0284	0.0400	0.0171	0.0301	0.0120	0.0237	0.0168	0.0298	0.0117	0.0234
	ASDBT	0.0346	0.0492	0.0284	0.0400	0.0171	0.0301	0.0120	0.0237	0.0168	0.0298	0.0117	0.0234
2	EBBT	0.0180	0.0343	0.0122	0.0261	0.0180	0.0343	0.0122	0.0261	0.0180	0.0343	0.0122	0.0261
	FSDBT	0.0910	0.1044	0.0848	0.0971	0.0201	0.0363	0.0142	0.0281	0.0187	0.0350	0.0129	0.0268
	PSDBT	0.0613	0.0827	0.0530	0.0682	0.0193	0.0357	0.0134	0.0273	0.0184	0.0348	0.0126	0.0265
	TSDBT	0.0611	0.0829	0.0531	0.0680	0.0193	0.0357	0.0134	0.0273	0.0184	0.0348	0.0126	0.0265
	HSDBT	0.0613	0.0827	0.0530	0.0681	0.0193	0.0357	0.0134	0.0273	0.0184	0.0348	0.0126	0.0265
	ESDBT	0.0603	0.0826	0.0525	0.0673	0.0192	0.0357	0.0134	0.0273	0.0184	0.0348	0.0126	0.0265
	ASDBT	0.0603	0.0826	0.0525	0.0673	0.0192	0.0357	0.0134	0.0273	0.0184	0.0348	0.0126	0.0265
4	EBBT	0.0184	0.0357	0.0124	0.0269	0.0184	0.0357	0.0124	0.0269	0.0184	0.0357	0.0124	0.0269
	FSDBT	0.0942	0.1100	0.0873	0.1014	0.0205	0.0378	0.0144	0.0290	0.0191	0.0365	0.0131	0.0276
	PSDBT	0.0810	0.1052	0.0735	0.0888	0.0202	0.0377	0.0142	0.0287	0.0190	0.0364	0.0130	0.0275
	TSDBT	0.0804	0.1055	0.0730	0.0882	0.0202	0.0377	0.0142	0.0287	0.0190	0.0365	0.0130	0.0276
	HSDBT	0.0810	0.1052	0.0736	0.0888	0.0202	0.0377	0.0142	0.0287	0.0190	0.0364	0.0130	0.0275
	ESDBT	0.0794	0.1053	0.0720	0.0872	0.0202	0.0377	0.0142	0.0287	0.0190	0.0365	0.0130	0.0275
	ASDBT	0.0794	0.1053	0.0720	0.0872	0.0202	0.0377	0.0142	0.0287	0.0190	0.0365	0.0130	0.0275
8	EBBT	0.0185	0.0361	0.0124	0.0271	0.0185	0.0361	0.0124	0.0271	0.0185	0.0361	0.0124	0.0271
	FSDBT	0.0951	0.1115	0.0880	0.1026	0.0206	0.0382	0.0145	0.0292	0.0192	0.0369	0.0132	0.0279
	PSDBT	0.0887	0.1136	0.0821	0.0969	0.0205	0.0383	0.0145	0.0291	0.0192	0.0369	0.0131	0.0278
	TSDBT	0.0879	0.1139	0.0812	0.0961	0.0205	0.0383	0.0145	0.0291	0.0192	0.0369	0.0131	0.0278
	HSDBT	0.0888	0.1135	0.0822	0.0969	0.0205	0.0383	0.0145	0.0291	0.0192	0.0369	0.0131	0.0278
	ESDBT	0.0868	0.1139	0.0800	0.0950	0.0205	0.0383	0.0144	0.0291	0.0192	0.0369	0.0131	0.0278
	ASDBT	0.0868	0.1139	0.0800	0.0950	0.0205	0.0383	0.0144	0.0291	0.0192	0.0369	0.0131	0.0278
10	EBBT	0.0185	0.0362	0.0124	0.0271	0.0185	0.0362	0.0124	0.0271	0.0185	0.0362	0.0124	0.0271
	FSDBT	0.0952	0.1117	0.0880	0.1027	0.0206	0.0383	0.0145	0.0292	0.0192	0.0369	0.0132	0.0279
	PSDBT	0.0898	0.1147	0.0833	0.0980	0.0206	0.0384	0.0145	0.0292	0.0192	0.0370	0.0132	0.0279
	TSDBT	0.0890	0.1150	0.0823	0.0972	0.0205	0.0384	0.0145	0.0292	0.0192	0.0370	0.0132	0.0279
	HSDBT	0.0899	0.1147	0.0833	0.0980	0.0206	0.0384	0.0145	0.0292	0.0192	0.0370	0.0132	0.0279
	ESDBT	0.0878	0.1150	0.0811	0.0961	0.0205	0.0384	0.0145	0.0292	0.0192	0.0370	0.0132	0.0279
	ASDBT	0.0878	0.1150	0.0811	0.0961	0.0205	0.0384	0.0145	0.0292	0.0192	0.0370	0.0132	0.0279
CET	EBBT	0.0185	0.0362	0.0124	0.0272	0.0185	0.0362	0.0124	0.0272	0.0185	0.0362	0.0124	0.0272
	FSDBT	0.0954	0.1120	0.0882	0.1030	0.0206	0.0383	0.0145	0.0293	0.0193	0.0370	0.0132	0.0279
	PSDBT	0.0917	0.1168	0.0855	0.1000	0.0206	0.0385	0.0146	0.0293	0.0193	0.0371	0.0132	0.0279

h/l	Model	L/h=5				L/h=30				L/h=50			
		UD	FG-O	FG-X	FG-V	UD	FG-O	FG-X	FG-V	UD	FG-O	FG-X	FG-V
	TSDBT	0.0908	0.1171	0.0844	0.0992	0.0206	0.0385	0.0146	0.0293	0.0193	0.0371	0.0132	0.0279
	HSDBT	0.0918	0.1167	0.0856	0.1001	0.0206	0.0385	0.0146	0.0293	0.0193	0.0371	0.0132	0.0279
	ESDBT	0.0896	0.1171	0.0831	0.0980	0.0206	0.0386	0.0146	0.0293	0.0193	0.0371	0.0132	0.0279
	ASDBT	0.0896	0.1171	0.0831	0.0980	0.0206	0.0386	0.0146	0.0293	0.0193	0.0371	0.0132	0.0279

Table 9. Maximum dimensionless deflection (\bar{w}) of FG-CNTRC microbeams under sinusoidal load ($V_{CNT}^* = 0.17$ and with elastic foundation $K_w = 10$, $K_p = 5$)

h/l	Model	L/h=5				L/h=30				L/h=50			
		UD	FG-O	FG-X	FG-V	UD	FG-O	FG-X	FG-V	UD	FG-O	FG-X	FG-V
1	EBBT	0.0164	0.0290	0.0114	0.0229	0.0164	0.0290	0.0114	0.0229	0.0164	0.0290	0.0114	0.0229
	FSDBT	0.0766	0.0832	0.0728	0.0796	0.0183	0.0307	0.0134	0.0247	0.0171	0.0296	0.0121	0.0236
	PSDBT	0.0342	0.0480	0.0278	0.0393	0.0170	0.0296	0.0119	0.0234	0.0166	0.0292	0.0116	0.0231
	TSDBT	0.0342	0.0481	0.0280	0.0394	0.0170	0.0296	0.0119	0.0234	0.0166	0.0292	0.0116	0.0231
	HSDBT	0.0342	0.0480	0.0278	0.0393	0.0170	0.0296	0.0119	0.0234	0.0166	0.0292	0.0116	0.0231
	ESDBT	0.0339	0.0478	0.0279	0.0391	0.0170	0.0296	0.0119	0.0234	0.0166	0.0292	0.0116	0.0231
	ASDBT	0.0339	0.0478	0.0279	0.0391	0.0170	0.0296	0.0119	0.0234	0.0166	0.0292	0.0116	0.0231
2	EBBT	0.0178	0.0336	0.0121	0.0257	0.0178	0.0336	0.0121	0.0257	0.0178	0.0336	0.0121	0.0257
	FSDBT	0.0863	0.0984	0.0807	0.0918	0.0198	0.0355	0.0141	0.0276	0.0185	0.0343	0.0128	0.0264
	PSDBT	0.0591	0.0789	0.0514	0.0655	0.0190	0.0350	0.0133	0.0269	0.0182	0.0341	0.0125	0.0261
	TSDBT	0.0590	0.0791	0.0514	0.0654	0.0190	0.0350	0.0133	0.0269	0.0182	0.0341	0.0125	0.0261
	HSDBT	0.0591	0.0788	0.0514	0.0655	0.0190	0.0350	0.0133	0.0269	0.0182	0.0341	0.0125	0.0261
	ESDBT	0.0583	0.0787	0.0509	0.0647	0.0190	0.0350	0.0133	0.0269	0.0182	0.0341	0.0125	0.0261
	ASDBT	0.0583	0.0787	0.0509	0.0647	0.0190	0.0350	0.0133	0.0269	0.0182	0.0341	0.0125	0.0261
4	EBBT	0.0182	0.0350	0.0123	0.0265	0.0182	0.0350	0.0123	0.0265	0.0182	0.0350	0.0123	0.0265
	FSDBT	0.0892	0.1033	0.0830	0.0957	0.0202	0.0370	0.0143	0.0285	0.0189	0.0357	0.0130	0.0272
	PSDBT	0.0773	0.0990	0.0705	0.0843	0.0200	0.0369	0.0140	0.0282	0.0188	0.0357	0.0129	0.0271
	TSDBT	0.0768	0.0993	0.0700	0.0838	0.0200	0.0369	0.0140	0.0282	0.0188	0.0357	0.0129	0.0271
	HSDBT	0.0773	0.0990	0.0705	0.0843	0.0200	0.0369	0.0140	0.0282	0.0188	0.0357	0.0129	0.0271
	ESDBT	0.0758	0.0991	0.0690	0.0830	0.0199	0.0369	0.0140	0.0282	0.0188	0.0357	0.0129	0.0271
	ASDBT	0.0758	0.0991	0.0690	0.0830	0.0199	0.0369	0.0140	0.0282	0.0188	0.0357	0.0129	0.0271
8	EBBT	0.0183	0.0354	0.0123	0.0267	0.0183	0.0354	0.0123	0.0267	0.0183	0.0354	0.0123	0.0267
	FSDBT	0.0900	0.1046	0.0836	0.0967	0.0203	0.0374	0.0144	0.0287	0.0190	0.0361	0.0131	0.0274
	PSDBT	0.0843	0.1064	0.0783	0.0916	0.0203	0.0375	0.0143	0.0286	0.0190	0.0361	0.0130	0.0274
	TSDBT	0.0836	0.1067	0.0775	0.0909	0.0203	0.0375	0.0143	0.0286	0.0190	0.0361	0.0130	0.0274
	HSDBT	0.0844	0.1064	0.0783	0.0916	0.0203	0.0375	0.0143	0.0286	0.0190	0.0361	0.0130	0.0274
	ESDBT	0.0825	0.1066	0.0763	0.0899	0.0203	0.0375	0.0143	0.0286	0.0190	0.0361	0.0130	0.0274
	ASDBT	0.0825	0.1066	0.0763	0.0899	0.0203	0.0375	0.0143	0.0286	0.0190	0.0361	0.0130	0.0274
10	EBBT	0.0183	0.0354	0.0123	0.0267	0.0183	0.0354	0.0123	0.0267	0.0183	0.0354	0.0123	0.0267
	FSDBT	0.0901	0.1047	0.0837	0.0968	0.0204	0.0374	0.0144	0.0287	0.0190	0.0361	0.0131	0.0274
	PSDBT	0.0853	0.1074	0.0794	0.0926	0.0203	0.0375	0.0144	0.0287	0.0190	0.0362	0.0131	0.0274
	TSDBT	0.0845	0.1077	0.0785	0.0919	0.0203	0.0375	0.0144	0.0287	0.0190	0.0362	0.0131	0.0274
	HSDBT	0.0853	0.1074	0.0794	0.0926	0.0203	0.0375	0.0144	0.0287	0.0190	0.0362	0.0131	0.0274
	ESDBT	0.0834	0.1077	0.0773	0.0909	0.0203	0.0376	0.0144	0.0287	0.0190	0.0362	0.0131	0.0274
	ASDBT	0.0834	0.1077	0.0773	0.0909	0.0203	0.0376	0.0144	0.0287	0.0190	0.0362	0.0131	0.0274
CET	EBBT	0.0183	0.0355	0.0123	0.0268	0.0183	0.0355	0.0123	0.0268	0.0183	0.0355	0.0123	0.0268
	FSDBT	0.0903	0.1050	0.0838	0.0970	0.0204	0.0375	0.0144	0.0288	0.0190	0.0362	0.0131	0.0275
	PSDBT	0.0870	0.1092	0.0814	0.0944	0.0204	0.0377	0.0144	0.0288	0.0190	0.0363	0.0131	0.0275
	TSDBT	0.0862	0.1095	0.0804	0.0936	0.0204	0.0377	0.0144	0.0288	0.0190	0.0363	0.0131	0.0275
	HSDBT	0.0871	0.1092	0.0814	0.0945	0.0204	0.0377	0.0144	0.0288	0.0190	0.0363	0.0131	0.0275
	ESDBT	0.0851	0.1095	0.0792	0.0926	0.0204	0.0377	0.0144	0.0288	0.0190	0.0363	0.0131	0.0275
	ASDBT	0.0851	0.1095	0.0792	0.0926	0.0204	0.0377	0.0144	0.0288	0.0190	0.0363	0.0131	0.0275

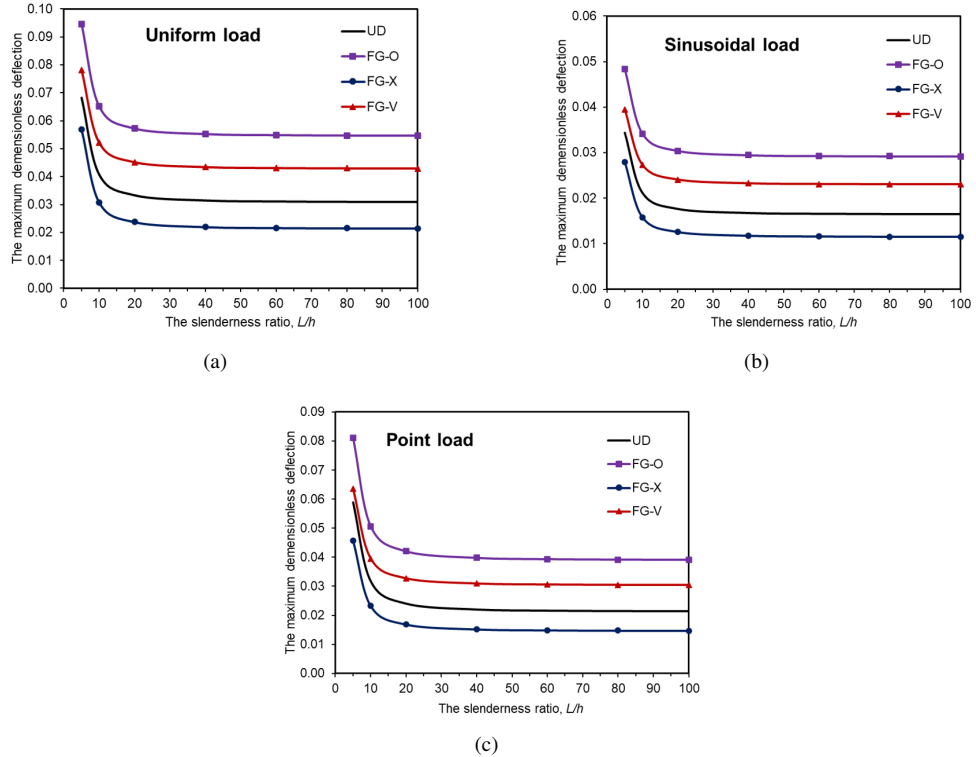


Figure 8. Maximum dimensionless deflections (\bar{w}) of FG-CNTRC microbeams resting on elastic foundation with the slenderness ratio (L/h)

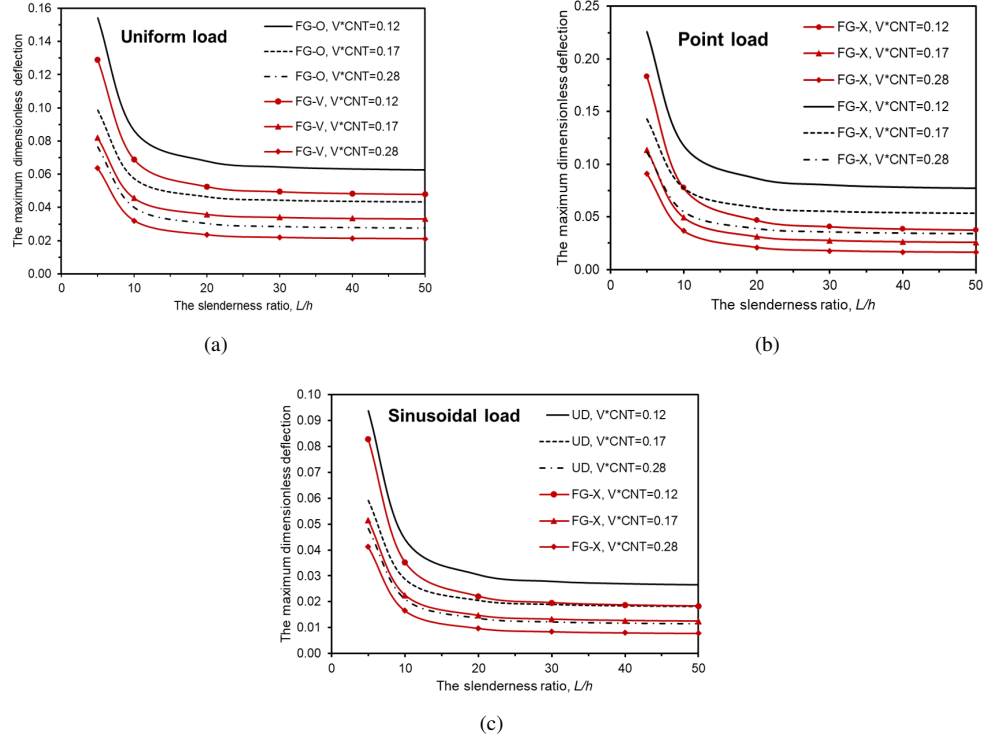


Figure 9. Impact of the CNT volume fraction V^*_{CNT} on the static bending behavior of FG-CNTRC microbeams resting on elastic foundation

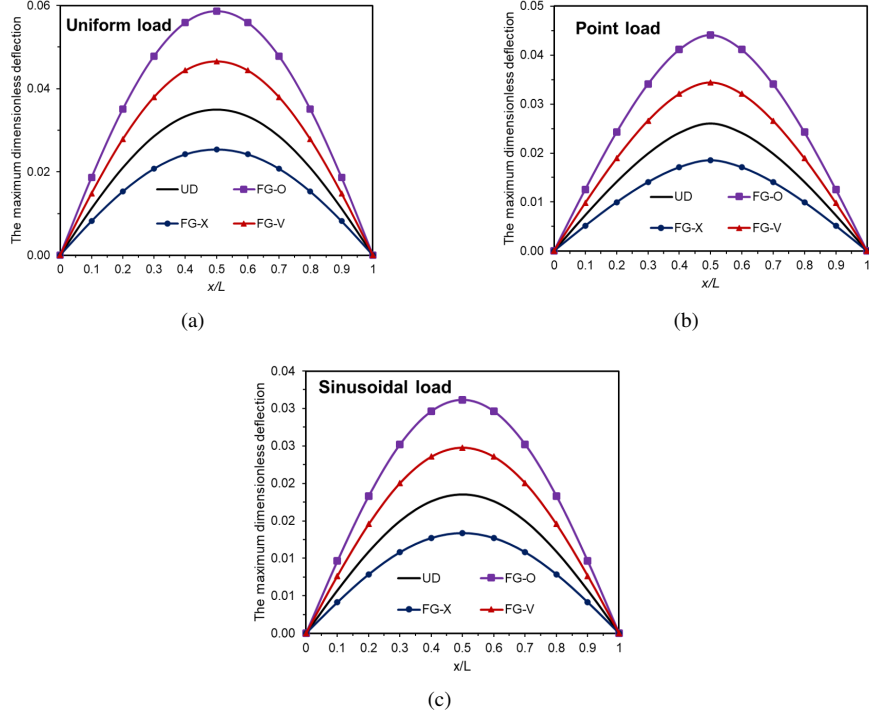


Figure 10. Maximum dimensionless deflections (\bar{w}) of FG-CNTRC microbeams resting on elastic foundation to the normalized microbeam length (x/L)

7 Conclusions

This study conducted a detailed analytical investigation into the static bending behaviour of FG-CNTRC microbeams on elastic foundations by coupling the higher-order shear deformation beam theory (HoSDBT) with the modified couple stress theory (MCST). The key findings not only confirmed the expected trends but also yielded actionable engineering insights as follows:

- The inclusion of the material length-scale parameter via the MCST enables the prediction of significantly higher bending stiffness when the microbeam thickness approaches the intrinsic material length. Engineering insight: For ultra-thin microbeam design, neglecting size-effects may result in conservative stiffness estimates; incorporating the MCST allows slimmer designs with confidence in reliability.
- Increasing the CNT volume fraction and adopting favourable gradation schemes (e.g., UD, FG-O, FG-X, and FG-V) lead to substantial reductions in deflection. Engineering insight: When specifying FG-CNTRC microbeams for load-bearing applications, choosing gradation profiles with greater reinforcement at outer layers (e.g., FG-X) is directly beneficial in enhancing stiffness and reducing deformation without necessarily increasing the total volume fraction.
- While the CNT gradation profile influences the absolute structural response, the overarching trend remains: FG-O yields the lowest stiffness, FG-X the highest, with FG-V and UD in between. Engineering insight: This ranking provides design practitioners with a clear hierarchy of gradation effectiveness, so as to enable informed selection of material configuration depending on budget, manufacturability, and performance target.
- Both the Winkler and Pasternak foundation models significantly affect mechanical response: the Winkler foundation produces gradually increasing stiffness whereas the Pasternak model with shear coupling drives more pronounced stiffness gains. Engineering insight: In micro-device design where foundation interaction is present (e.g., microbeams embedded in elastic substrates or coatings), using a foundation model with shear coupling (Pasternak type) may better capture the enhancement of stiffness. This suggests that for realistic device modelling and optimization, the choice of foundation modelling cannot be neglected.

In summary, the integrated MCST-enhanced HoSDBT framework constitutes a robust analytical tool that encapsulates size-effect, CNT volume fraction and gradation, and foundation stiffness in a unified model. For design engineers, it offers a direct pathway to tailor microbeam configurations (thickness, CNT distribution, and foundation support) to meet specific stiffness and deformation requirements, thus bridging rigorous theoretical modelling with practical implementation.

Looking ahead, further work could extend this framework to dynamic loading (vibration and fatigue), thermal

environments, and multifunctional behaviour (e.g., piezo-electric coupling). These extensions will further enhance the applicability of the model in the development of resilient and high-performance FG–CNTRC micro-devices across advanced engineering domains.

Data Availability

The data used to support the findings of this study are available from the corresponding author upon request.

Conflicts of Interest

The author declares that they have no conflicts of interest.

References

- [1] N. Hossain, M. Z. A. Mahmud, A. Hossain, M. K. Rahman, M. S. Islam, R. Tasnim, and M. H. Mobarak, “Advances of materials science in MEMS applications: A review,” *Results Eng.*, vol. 22, p. 102115, 2024. <https://doi.org/10.1016/j.rineng.2024.102115>
- [2] I. Stachiv, E. Alarcon, and M. Lamac, “Shape memory alloys and polymers for MEMS/NEMS applications: Review on recent findings and challenges in design, preparation, and characterization,” *Metals*, vol. 11, no. 3, p. 415, 2021. <https://doi.org/10.3390/met11030415>
- [3] B. Padha, I. Yadav, S. Dutta, and S. Arya, “Recent developments in wearable NEMS/MEMS-based smart infrared sensors for healthcare applications,” *ACS Appl. Electron. Mater.*, vol. 5, no. 10, pp. 5386–5411, 2023. <https://doi.org/10.1021/acsaelm.3c00860>
- [4] X. Fan, C. He, J. Ding, Q. Gao, H. Ma, M. C. Lemme, and W. Zhang, “Graphene MEMS and NEMS,” *Microsyst. Nanoeng.*, vol. 10, p. 154, 2024. <https://doi.org/10.1038/s41378-024-00791-5>
- [5] W. C. Chuang, H. L. Lee, P. Z. Chang, and Y. C. Hu, “Review on the modeling of electrostatic MEMS,” *Sensors*, vol. 10, pp. 6149–6171, 2010. <https://doi.org/10.3390/s100606149>
- [6] E. Garcia, N. Lobontiu, and Y. Nam, “Mechanics of MEMS: A review of modeling, analysis, and design,” *Proc. SPIE*, vol. 5390, 2004. <https://doi.org/10.1117/12.540070>
- [7] W. M. Zhang, H. Yan, Z. K. Peng, and G. Meng, “Electrostatic pull-in instability in MEMS/NEMS: A review,” *Sens. Actuators A Phys.*, vol. 214, pp. 187–218, 2014. <https://doi.org/10.1016/j.sna.2014.04.025>
- [8] M. Naebe and K. Shirvanimoghaddam, “Functionally graded materials: A review of fabrication and properties,” *Appl. Mater. Today*, vol. 5, pp. 223–245, 2016. <https://doi.org/10.1016/j.apmt.2016.10.001>
- [9] B. Saleh, J. Jiang, R. Fathi, T. Al-hababi, Q. Xu, L. Wang, D. Song, and A. Ma, “30 years of functionally graded materials: An overview of manufacturing methods, applications and future challenges,” *Compos. B Eng.*, vol. 201, p. 108376, 2020. <https://doi.org/10.1016/j.compositesb.2020.108376>
- [10] S. Iijima, “Helical microtubules of graphitic carbon,” *Nature*, vol. 354, no. 6348, pp. 56–58, 1991. <https://doi.org/10.1038/354056a0>
- [11] A. K. Gartia and S. Chakraverty, “Advanced computational modeling and mechanical behavior analysis of multi-directional functionally graded nanostructures: A comprehensive review,” *Comput. Model. Eng. Sci.*, vol. 142, no. 3, pp. 2405–2455, 2025. <https://doi.org/10.32604/cmes.2025.061039>
- [12] H. Haghshenas Gorgani, M. Mahdavi Adeli, and M. Hosseini, “Pull-in behavior of functionally graded micro/nano-beams for MEMS and NEMS switches,” *Microsyst. Technol.*, vol. 25, pp. 3165–3173, 2019. <https://doi.org/10.1007/s00542-018-4216-4>
- [13] A. Shariati, D. W. Jung, H. Mohammad-Sedighi, K. K. Žur, M. Habibi, and M. Safa, “Stability and dynamics of viscoelastic moving rayleigh beams with an asymmetrical distribution of material parameters,” *Symmetry*, vol. 12, p. 586, 2020. <https://doi.org/10.3390/sym12040586>
- [14] L. Hadji, V. Plevris, and G. Papazafeiropoulos, “Investigation of the static bending response of FGM sandwich plates,” *J. Appl. Comput. Mech.*, vol. 10, no. 1, pp. 26–37, 2024. <https://doi.org/10.22055/jacm.2023.44278.4194>
- [15] V. Rizov, “The effect of delamination between layers in U-shaped members made of functionally graded multilayered viscoelastic materials,” *J. Appl. Comput. Mech.*, vol. 10, no. 4, pp. 830–841, 2024. <https://doi.org/10.22055/jacm.2024.46014.4449>
- [16] H. S. Shen, “Nonlinear bending of functionally graded carbon nanotube reinforced composite plates in thermal environments,” *Compos. Struct.*, vol. 91, pp. 9–19, 2009. <https://doi.org/10.1016/j.compstruct.2009.04.026>
- [17] K. M. Liew, Z. X. Lei, and L. W. Zhang, “Mechanical analysis of functionally graded carbon nanotube reinforced composites: A review,” *Compos. Struct.*, vol. 120, pp. 90–97, 2015. <https://doi.org/10.1016/j.compstruct.2014.09.041>
- [18] L. L. Ke, J. Yang, and S. Kitipornchai, “Nonlinear free vibration of functionally graded carbon nanotube-reinforced composite beams,” *Compos. Struct.*, vol. 92, no. 3, pp. 676–683, 2010. <https://doi.org/10.1016/j.compositesb.2009.09.024>

- [19] F. Lin and Y. Xiang, "Vibration of carbon nanotube reinforced composite beams based on the first and third order beam theories," *Appl. Math. Model.*, vol. 38, no. 15–16, pp. 3741–3754, 2014. <https://doi.org/10.1016/j.apm.2014.02.008>
- [20] H. S. Shen and Y. Xiang, "Nonlinear analysis of nanotube-reinforced composite beams resting on elastic foundations in thermal environments," *Eng. Struct.*, vol. 56, pp. 698–708, 2013. <https://doi.org/10.1016/j.engstruct.2013.06.002>
- [21] R. Ansari, M. F. Shojaei, V. Mohammadi, R. Gholami, and F. Sadeghi, "Nonlinear forced vibration analysis of functionally graded carbon nanotube-reinforced composite Timoshenko beams," *Compos. Struct.*, vol. 113, pp. 316–327, 2014. <https://doi.org/10.1016/j.compstruct.2014.03.015>
- [22] Z. Shi, X. Yao, F. Pang, and Q. Wang, "An exact solution for the free-vibration analysis of functionally graded carbon-nanotube-reinforced composite beams with arbitrary boundary conditions," *Sci. Rep.*, vol. 7, p. 12909, 2017. <https://doi.org/10.1038/s41598-017-12596-w>
- [23] N. Wattanasakulpong and V. Ungbhakorn, "Analytical solutions for bending, buckling and vibration responses of carbon nanotube-reinforced composite beams resting on elastic foundation," *Comput. Mater. Sci.*, vol. 71, pp. 201–208, 2013. <https://doi.org/10.1016/j.commatsci.2013.01.028>
- [24] J. S. Stölken and A. G. Evans, "A microbend test method for measuring the plasticity length scale," *Acta Mater.*, vol. 46, no. 14, pp. 5109–5115, 1998. [https://doi.org/10.1016/S1359-6454\(98\)00153-0](https://doi.org/10.1016/S1359-6454(98)00153-0)
- [25] Z. F. Shi, B. Huang, H. Tan, Y. Huang, T. Y. Zhang, P. D. Wu, K. C. Hwang, and H. Gao, "Determination of the microscale stress-strain curve and strain gradient effect from the micro-bend of ultra-thin beams," *Int. J. Plast.*, vol. 24, no. 9, pp. 1606–1624, 2008. <https://doi.org/10.1016/j.ijplas.2007.12.007>
- [26] A. C. Eringen, "Linear theory of nonlocal elasticity and dispersion of plane waves," *Int. J. Eng. Sci.*, vol. 10, pp. 425–435, 1972. [https://doi.org/10.1016/0020-7225\(72\)90050-X](https://doi.org/10.1016/0020-7225(72)90050-X)
- [27] A. C. Eringen, "On differential equations of nonlocal elasticity and solutions of screw dislocation and surface waves," *J. Appl. Phys.*, vol. 54, pp. 4703–4710, 1983. <https://doi.org/10.1063/1.332803>
- [28] R. D. Mindlin, "Micro-structure in linear elasticity," *Arch. Ration. Mech. Anal.*, vol. 16, pp. 51–78, 1964. <https://doi.org/10.1007/BF00248490>
- [29] R. D. Mindlin, "Second gradient of strain and surface-tension in linear elasticity," *Int. J. Solids Struct.*, vol. 1, no. 4, pp. 417–438, 1965. [https://doi.org/10.1016/0020-7683\(65\)90006-5](https://doi.org/10.1016/0020-7683(65)90006-5)
- [30] R. A. Toupin, "Elastic materials with couple-stresses," *Arch. Ration. Mech. Anal.*, vol. 11, pp. 385–414, 1962. <https://doi.org/10.1007/BF00253945>
- [31] W. T. Koiter, "Couple stresses in the theory of elasticity, i and ii," *Proc. K. Ned. Akad. Wet. B*, vol. 67, pp. 17–44, 1964.
- [32] F. Yang, A. C. M. Chong, D. C. C. Lam, and P. Tong, "Couple stress based strain gradient theory for elasticity," *Int. J. Solids Struct.*, vol. 39, no. 10, pp. 2731–2743, 2002. [https://doi.org/10.1016/S0020-7683\(02\)00152-X](https://doi.org/10.1016/S0020-7683(02)00152-X)
- [33] C. W. Lim, G. Zhang, and J. N. Reddy, "A higher-order nonlocal elasticity and strain gradient theory and its applications in wave propagation," *J. Mech. Phys. Solids*, vol. 78, pp. 298–313, 2015. <https://doi.org/10.1016/j.jmps.2015.02.001>
- [34] H. T. Thai, T. P. Vo, T. K. Nguyen, and S. E. Kim, "A review of continuum mechanics models for size-dependent analysis of beams and plates," *Compos. Struct.*, vol. 177, pp. 196–219, 2017. <https://doi.org/10.1016/j.compstruct.2017.06.040>
- [35] F. Ebrahimi and M. R. Barati, "A nonlocal higher-order shear deformation beam theory for vibration analysis of size-dependent functionally graded nanobeams," *Arab. J. Sci. Eng.*, vol. 41, pp. 1679–1690, 2016. <https://doi.org/10.1007/s13369-015-1930-4>
- [36] A. Shariati, D. W. Jung, H. Mohammad-Sedighi, K. K. Žur, M. Habibi, and M. Safa, "On the vibrations and stability of moving viscoelastic axially functionally graded nanobeams," *Mater.*, vol. 13, no. 7, p. 1707, 2020. <https://doi.org/10.3390/ma13071707>
- [37] S. Kong, "A review on the size-dependent models of micro-beam and micro-plate based on the modified couple stress theory," *Arch. Comput. Methods Eng.*, vol. 29, pp. 1–31, 2022. <https://doi.org/10.1007/s11831-021-09567-w>
- [38] M. Simsek and J. N. Reddy, "Bending and vibration of functionally graded microbeams using a new higher order beam theory and the modified couple stress theory," *Int. J. Eng. Sci.*, vol. 64, pp. 37–53, 2013. <https://doi.org/10.1016/j.ijengsci.2012.12.002>
- [39] L. L. Ke and Y. S. Wang, "Size effect on dynamic stability of functionally graded microbeams based on a modified couple stress theory," *Compos. Struct.*, vol. 93, no. 2, pp. 342–350, 2011. <https://doi.org/10.1016/j.compstruct.2010.09.008>
- [40] M. Gorji Azandariani, M. Gholami, E. Vaziri, and A. Nikzad, "Nonlinear static analysis of a bi-directional

- functionally graded microbeam based on a nonlinear elastic foundation using modified couple stress theory,” *Arab. J. Sci. Eng.*, vol. 46, pp. 12 641–12 651, 2021. <https://doi.org/10.1007/s13369-021-06053-0>
- [41] N. Wattanasakulpong, A. Chaikittiratana, and S. Pornpeerakeat, “Vibration of size-dependent functionally graded sandwich microbeams with different boundary conditions based on the modified couple stress theory,” *J. Sandwich Struct. Mater.*, vol. 22, no. 2, pp. 220–247, 2017. <https://doi.org/10.1177/10996362177389>
- [42] G. A. Shenas, S. Ziaeef, and P. Malekzadeh, “A unified higher-order beam theory for free vibration and buckling of FG-CNT reinforced microbeams embedded in elastic medium based on unifying stress–strain gradient framework,” *Iran. J. Sci. Technol. Trans. Mech. Eng.*, vol. 43, pp. 469–492, 2019. <https://doi.org/10.1007/s40997-018-0171-z>
- [43] M. Alimoradzadeh, H. Heidari, F. Tornabene, and R. Dimitri, “Nonlinear dynamic study of non-uniform microscale CNTR composite beams based on a modified couple stress theory,” *Int. J. Non-Linear Mech.*, vol. 156, p. 104477, 2023. <https://doi.org/10.1016/j.ijnonlinmec.2023.104477>
- [44] M. A. Khorshidi, “The material length scale parameter used in couple stress theories is not a material constant,” *Int. J. Eng. Sci.*, vol. 133, pp. 15–25, 2018. <https://doi.org/10.1016/j.ijengsci.2018.08.005>